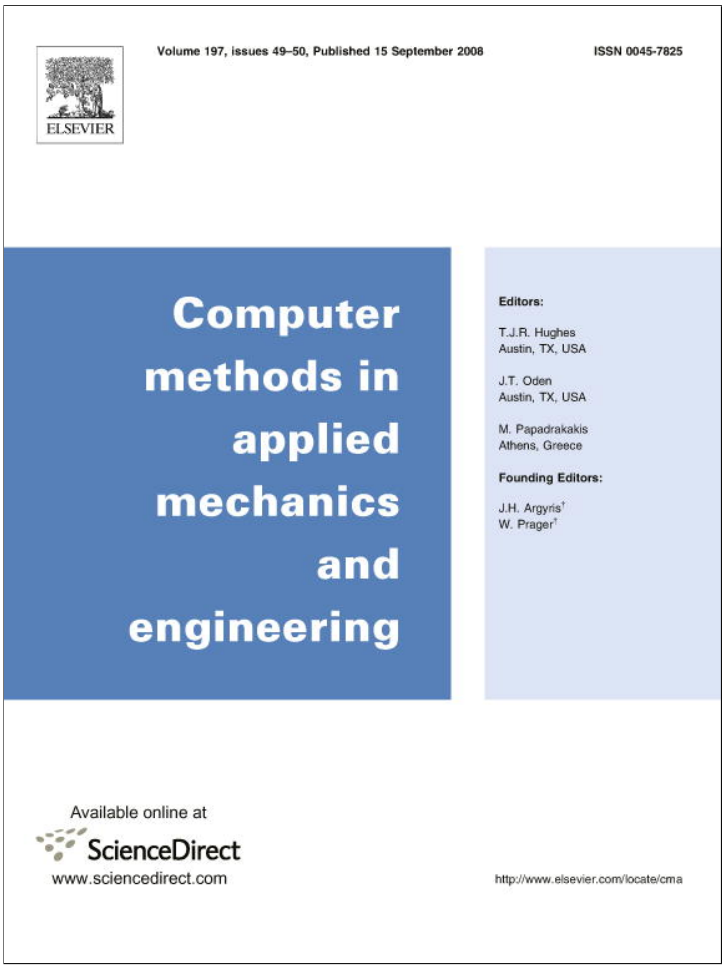

Comput. Methods Appl. Mech. Engrg. 197 (2008) 4307–4318

Contents lists available at ScienceDirect

Comput. Methods Appl. Mech. Engrg.

journal homepage: www.elsevier.com/locate/cma

# Interior superconvergence in mortar and non-mortar mixed finite element methods on non-matching grids

Gergina Pencheva [a,*], Ivan Yotov [b]

[a] Center for Subsurface Modeling, Institute for Computational Engineering and Sciences, The University of Texas at Austin, Austin, TX 78712, United States
[b] Department of Mathematics, 301 Thackeray Hall, University of Pittsburgh, Pittsburgh, PA 15260, United States

ARTICLE INFO

*Article history:*
Received 29 August 2007
Received in revised form 14 February 2008
Accepted 6 May 2008
Available online 23 May 2008

*Keywords:*
Mixed finite element
Mortar finite element
Interior estimates
Superconvergence
Non-matching grids

ABSTRACT

We establish interior velocity superconvergence estimates for mixed finite element approximations of second order elliptic problems on non-matching rectangular and quadrilateral grids. Both mortar and non-mortar methods for imposing the interface conditions are considered. In both cases it is shown that a discrete $L^2$-error in the velocity in a compactly contained subdomain away from the interfaces converges of order $\mathcal{O}(h^{1/2})$ higher than the error in the whole domain. For the non-mortar method we also establish pressure superconvergence, which is needed in the velocity analysis. Numerical results are presented in confirmation of the theory.



## 1. Introduction

The use of non-matching multiblock grids in discretizations of partial differential equations provides great flexibility in meshing highly irregular domains and accurately handling internal features, e.g., faults and geological layers in porous media. At the same time, special care has to be taken to impose properly interface continuity conditions. The computational error due to the non-matching grids affects the overall accuracy of the solution. In this paper we study how this interface error propagates into the interior of the subdomains.

We consider the second order elliptic equation written as a first order system

$$\mathbf{u} = -K\nabla p \quad \text{in } \Omega, \tag{1.1}$$

$$\nabla \cdot \mathbf{u} = f \quad \text{in } \Omega, \tag{1.2}$$

$$p = g \quad \text{on } \partial\Omega, \tag{1.3}$$

where $\Omega \subset \mathbb{R}^d$, $d = 2$ or 3, and $K$ is a symmetric, uniformly positive definite tensor with $L^\infty(\Omega)$ components. The above system models single-phase flow in porous media among many other applications. Here $p$ is the pressure, $\mathbf{u}$ is the Darcy velocity, and $K$ represents the rock permeability divided by the fluid viscosity. We assume that $K(\mathbf{x})$ satisfies

$$\forall \mathbf{x} \in \Omega, \quad k_0 \xi^T \xi \leqslant \xi^T K(\mathbf{x}) \xi \leqslant k_1 \xi^T \xi \quad \forall \xi \in \mathbb{R}^d. \tag{1.4}$$

The Dirichlet boundary conditions are considered merely for simplicity of the presentation. Neumann boundary conditions $\mathbf{u} \cdot \nu = g^N$ and Robin boundary conditions $-\alpha p + \mathbf{u} \cdot \nu = g^R$, where $\nu$ is the outward unit normal vector on $\partial\Omega$, can also be considered. We assume that the problem (1.1)–(1.3) is $H^2$-regular, i.e., there exists a positive constant $C$ depending only on $K$ and $\Omega$ such that

$$\|p\|_2 \leqslant C(\|f\| + \|g\|_{3/2,\partial\Omega}), \tag{1.5}$$

where $H^2$ is the standard Hilbert space of functions having second order weak derivatives in $L^2$. Sufficient conditions for (1.5) are, for example, $K \in C^{0,1}(\overline{\Omega})$ and $\Omega$ is convex or $\partial\Omega$ is smooth enough [20,22].

We study the approximation of (1.1)–(1.3) by mixed finite element methods on non-matching grids. Mixed methods are of interest due to their local mass conservation and high accuracy for both pressure and velocity, especially on structured grids. Multiblock discretizations allow for modeling highly irregular domains, while keeping the subdomain grids relatively simple. As a result, the use of mixed finite element subdomain discretizations can lead to accurate and efficient methods.

Continuity of flux and pressure must be imposed on interfaces. We consider two approaches, a mortar and a non-mortar method. In the mortar mixed finite element method [1,21,34] a mortar finite element pressure Lagrange multiplier is introduced on the interfaces to impose weakly continuity of flux. If the mortar space contains polynomials of degree one order higher than the traces of

* Corresponding author. Tel.: +1 512 475 8631; fax: +1 512 232 2445.
*E-mail addresses:* gergina@ices.utexas.edu (G. Pencheva), yotov@math.pitt.edu (I. Yotov).

0045-7825/$ - see front matter © 2008 Elsevier B.V. All rights reserved.
doi:10.1016/j.cma.2008.05.010

subdomain velocities, the method is optimally convergent and even superconvergent in certain cases [1,34]. We refer the reader to [6,7,16,23,33] for some examples of applications of mortar spaces to other types of discretizations.

In the non-mortar mixed finite element method [3], interface conditions are imposed without the use of a mortar space. On each subdomain, a partially hybridized mixed method is employed. Lagrange multiplier pressures are introduced on the element faces (or edges) on the subdomain interfaces $\Gamma$ as in [4,11,19]. Since the grids are non-matching across $\Gamma$, the Lagrange multipliers are double-valued. Robin type conditions are imposed on $\Gamma$ to couple the subdomain problems. The method has an advantage if adaptive local refinement techniques are to be used, since there is no mortar grid to refine. Such refinement could be difficult to implement in the mortar mixed method, since accuracy depends subtly on the relations between the mortar grid and the traces of the grids of the subdomain blocks [1], see the mortar condition (2.28).

In this paper we combine cutoff function and superconvergence techniques to establish interior error estimates for the velocity in mortar and non-mortar discretizations. We refer to [2,15,17,18,24] for relevant superconvergence results for mixed finite element methods on rectangular and quadrilateral elements. There are also examples of the use of cutoff functions in the context of mixed finite element methods. In [14], interior and superconvergence estimates are established in negative norms for linear and semi-linear elliptic problems. Interior estimates are established in [2] for a cell-centered finite difference version of the mixed method, as well as in [31] for an enhanced velocity mixed finite element method. Here we establish interior superconvergence for the velocity in mortar and non-mortar mixed finite element methods. For both methods, if the grids are rectangular or mildly distorted quadrilateral, we show that the velocity converges of order $\mathcal{O}(h^{1/2})$ higher in a compactly contained subdomain than in the whole domain. In the mortar case the superconvergence is the same as in single block discretizations with no boundary error. As a tool in the analysis we prove pressure superconvergence for the non-mortar method using a duality argument. Our analysis shows that the numerical error depends on the smoothness of the solution on every subdomain up to the interface. Numerical experiments confirm both the interior superconvergence for smooth solutions, as well as deterioration of interior convergence for singular solutions.

The remainder of the paper is organized as follows. In the next section, we recall the mortar and non-mortar mixed finite element methods and their convergence properties. Section 3 is devoted to the interior error analysis for the mortar method. The non-mortar method is analyzed in Section 4. Numerical experiments confirming the theory are presented in Section 5.

## 2. Formulation of the methods and preliminaries

We will use the following standard notation. For $D \subset \mathbb{R}^d$, let $(\cdot,\cdot)$ and $\|\cdot\|_D$ be the $L^2(D)$ inner product and norm, respectively. Denote the norm in the Hilbert space $H^s(D)$ by $\|\cdot\|_{s,D}$. We may omit the subscript $D$ if $D=\Omega$. Similar notation is used for $S \subset \partial\Omega$, with the exception that the $L^2(S)$ inner product or duality pairing is denoted by $\langle\cdot,\cdot\rangle_S$. We denote by $c$ and $C$ generic positive constants, independent of the discretization parameter $h$.

The velocity and pressure functional spaces for the mixed weak formulation of (1.1)–(1.3) are defined as usual [11] to be

$$\mathbf{V} = H(\mathrm{div};\Omega) = \{\mathbf{v} \in (L^2(\Omega))^d : \nabla\cdot\mathbf{v} \in L^2(\Omega)\}, \quad W = L^2(\Omega),$$

with norms

$$\|\mathbf{v}\|_{\mathbf{V}} = (\|\mathbf{v}\|^2 + \|\nabla\cdot\mathbf{v}\|^2)^{1/2}, \quad \|w\|_W = \|w\|.$$

A weak solution of (1.1)–(1.3) is a pair $\mathbf{u} \in \mathbf{V}, p \in W$ such that

$$(K^{-1}\mathbf{u},\mathbf{v}) = (p,\nabla\cdot\mathbf{v}) - \langle g,\mathbf{v}\cdot\nu\rangle_{\partial\Omega}, \quad \mathbf{v} \in H(\mathrm{div};\Omega), \tag{2.1}$$

$$(\nabla\cdot\mathbf{u},w) = (f,w), \quad w \in L^2(\Omega). \tag{2.2}$$

It is well known (see, e.g., [11,28]) that (2.1)–(2.2) has a unique solution.

Let $\Omega$ be decomposed into non-overlapping subdomains (blocks) $\Omega_i$ so that $\overline{\Omega} = \cup_{i=1}^n \overline{\Omega}_i$ and $\Omega_i \cap \Omega_j = \emptyset$ for $i \neq j$. Let $\Gamma_{i,j} = \partial\Omega_i \cap \partial\Omega_j$ for $i \neq j$, $\Gamma_{i,i} = \emptyset$, $\Gamma = \cup_{1\leqslant i<j\leqslant n}\Gamma_{i,j}$, and $\Gamma_i = \partial\Omega_i \cap \Gamma = \partial\Omega_i \setminus \partial\Omega$ denote interior block interfaces. We assume that the interfaces are flat. The blocks need not share complete faces, i.e., they need not form a conforming partition. Denote by

$$\mathbf{V}_i = H(\mathrm{div};\Omega_i), \quad W_i = L^2(\Omega_i)$$

the subdomain functional spaces. To cast the problem (1.1)–(1.3) in a multiblock form, we write on each block $\Omega_i$

$$\mathbf{u} = -K\nabla p \quad \text{in } \Omega_i, \tag{2.3}$$

$$\nabla\cdot\mathbf{u} = f \quad \text{in } \Omega_i, \tag{2.4}$$

$$p = g \quad \text{on } \partial\Omega_i \cap \partial\Omega, \tag{2.5}$$

and on each interface $\Gamma_{i,j}$

$$p_i = p_j, \quad \mathbf{u}_i\cdot\nu_i + \mathbf{u}_j\cdot\nu_j = 0,$$

i.e., both the pressure and the flux are continuous across $\Gamma_{i,j}$. Here, $\nu_i$ is the outer unit normal to $\partial\Omega_i$ and for any $f$ defined on $\Omega$, we denote both $f|_{\Omega_k}$ and its trace $f|_{\Gamma_k}$ by $f_k$.

Let $\mathscr{T}_{h,i}$ be a conforming, shape-regular, quasi-uniform finite element partition of $\Omega_i, 1 \leqslant i \leqslant n$, of maximal element diameter $h_i$ [13]. To simplify the presentation, we let $h = \max_{1\leqslant i\leqslant n} h_i$ and analyze the methods in terms of this single value $h$. We allow for the possibility that the subdomain partitions $\mathscr{T}_{h,i}$ and $\mathscr{T}_{h,j}$ do not align on $\Gamma_{i,j}$. Define $\mathscr{T}_h = \cup_{i=1}^n \mathscr{T}_{h,i}$ and let

$$\mathbf{V}_{h,i} \times W_{h,i} \subset \mathbf{V}_i \times W_i$$

be any of the usual mixed finite element spaces defined on $\mathscr{T}_{h,i}$ (see [11, Section III.3]), the Raviart–Thomas (RT) spaces [27,25], the Brezzi–Douglas–Marini (BDM) spaces [10], the Brezzi–Douglas–Fortin–Marini (BDFM) spaces [9], the Brezzi–Douglas–Duràn–Fortin (BDDF) spaces [8], or the Chen–Douglas (CD) spaces [12]. We consider the above spaces on affine elements in $\mathbb{R}^2$ and $\mathbb{R}^3$ as well as RT and BDFM spaces on convex quadrilateral elements in $\mathbb{R}^2$. The order of the spaces is assumed to be the same on every subdomain. In the affine case, let $\mathbf{V}_{h,i}$ contain the polynomials of degree $k$ and $W_{h,i}$ contain the polynomials of degree $l$. For these spaces we have either $l=k$ or $l=k-1$, with the former true for RT and BDFM spaces. The mixed finite element spaces on quadrilaterals are defined via a transformation to the reference square $\widehat{E}$. For each element $E$, there exists a bijection mapping $F_E : \widehat{E} \to E$. Let $DF_E$ be the Jacobian matrix and let $J_E = |\det(DF_E)|$. If $\widehat{\mathbf{V}}(\widehat{E})$ and $\widehat{W}(\widehat{E})$ are the mixed finite element spaces on $\widehat{E}$, then the spaces on $E$ are defined via the transformations [29,11]

$$\mathbf{v} = \frac{1}{J_E} DF_E\hat{\mathbf{v}}\circ F_E^{-1}, \quad w = \hat{w}\circ F_E^{-1}.$$

The vector transformation is called the Piola transformation and preserves the normal components of the velocity vectors on the edges. It satisfies [11]

$$(\nabla\cdot\mathbf{v},w)_E = (\hat{\nabla}\cdot\hat{\mathbf{v}},\hat{w})_{\hat{E}}. \tag{2.6}$$

The pressure superconvergence result for the non-mortar method will be shown for all of the above spaces on affine elements in $\mathbb{R}^2$ and $\mathbb{R}^3$, as well as for the RT and BDFM spaces in $\mathbb{R}^2$ on $h^2$-parallelograms, see (2.7). Interior superconvergence of the velocity in

both methods will be shown for the RT and BDFM spaces on $h^2$-uniform quadrilateral grids, see (2.7)–(2.8), and, if $K$ is a diagonal tensor, on rectangular grids in $\mathbb{R}^3$.

Following the terminology from [18], a quadrilateral is called a $h^2$-parallelogram if it is a $h^2$-perturbation of a parallelogram:

$$\|(\mathbf{r}_2-\mathbf{r}_1)-(\mathbf{r}_3-\mathbf{r}_4)\|\leqslant Ch^2, \tag{2.7}$$

where $\mathbf{r}_i,\ i=1,\dots,4$, are the vertices of the quadrilateral, see Fig. 1. A quadrilateral partition is called $h^2$-uniform, if each element is a $h^2$-parallelogram and any two adjacent elements form a $h^2$-parallelogram, i.e.,

$$\|(\mathbf{r}_2-\mathbf{r}_1)-(\mathbf{r}'_2-\mathbf{r}'_1)\|\leqslant Ch^2, \tag{2.8}$$

where $\mathbf{r}'_i, i=1,\dots,4$, are the vertices of the adjacent element, see Fig. 1. We note that $h^2$-uniform grids can be constructed by uniform refinements of an initial quadrilateral grid or by smooth mapping of uniformly refined rectangular grids.

The velocity and pressure mixed finite element spaces on $\Omega$ are defined as follows:

$$\mathbf{V}_h=\bigoplus_{i=1}^{n}\mathbf{V}_{h,i},\quad W_h=\bigoplus_{i=1}^{n}W_{h,i}.$$

Note that the normal components of vectors in $\mathbf{V}_h$ are continuous between elements within each block $\Omega_i$, but not across $\Gamma$.

We introduce some projection operators needed in the analysis. For any of the standard mixed spaces there exists a projection operator $\Pi_i:(H^\epsilon(\Omega_i))^d\cap\mathbf{V}_i\to\mathbf{V}_{h,i}$ (for any $\varepsilon>0$), satisfying that for any $\mathbf{q}\in(H^\epsilon(\Omega_i))^d\cap\mathbf{V}_i$,

$$(\nabla\cdot(\Pi_i\mathbf{q}-\mathbf{q}),w)=0,\quad \forall\, w\in W_h, \tag{2.9}$$

$$\langle(\Pi_i\mathbf{q}-\mathbf{q})\cdot\nu_i,\mathbf{v}\cdot\nu_i\rangle_{\Gamma_i}=0,\quad \forall\mathbf{v}\in\mathbf{V}_{h,i}. \tag{2.10}$$

Define $\Pi:\oplus_{i=1}^n((H^\epsilon(\Omega_i))^d\cap\mathbf{V}_i)\to\mathbf{V}_h$ such that $\Pi|_{\Omega_i}=\Pi_i$. On affine elements,

$$\nabla\cdot\mathbf{V}_{h,i}=W_{h,i}. \tag{2.11}$$

On quadrilateral elements, (2.6) implies that on any element $E$

$$\nabla\cdot\mathbf{V}_{h,i}(E)=\frac{1}{J_E}W_{h,i}(E). \tag{2.12}$$

Since $J_E\neq$ constant, (2.11) does not hold for quadrilaterals.

Let $\widehat{Q}$ be the $L^2(\widehat{E})$-orthogonal projection onto $\widehat{W}(\widehat{E})$, satisfying for any $\hat{\varphi}\in L^2(\widehat{E})$,

$$(\hat{\varphi}-\widehat{Q}\hat{\varphi},\hat{w})=0,\quad \hat{w}\in\widehat{W}(\widehat{E}).$$

Let $Q_h:L^2(\Omega)\to W_h$ be the projection operator satisfying for any $\varphi\in L^2(\Omega)$,

$$Q_h\varphi=\widehat{Q}\hat{\varphi}\circ F_E^{-1}\quad\text{on all } E.$$

It is easy to see that, due to (2.6),

$$(\varphi-Q_h\varphi,\nabla\cdot\mathbf{v})=0,\quad\forall\,\mathbf{v}\in\mathbf{V}_h. \tag{2.13}$$

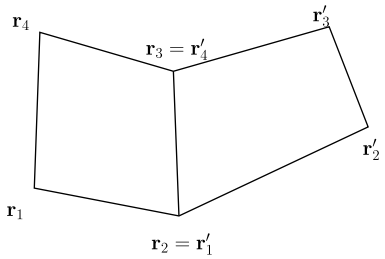


**Fig. 1.** $h^2$-Uniform quadrilateral grid.

For any $\phi\in L^2(\Gamma)$, let $\overline{\phi_i}\in\mathbf{V}_{h,i}\cdot\nu_i|_{\Gamma_i}$ be its $L^2(\Gamma_i)$-orthogonal projection satisfying

$$\langle\phi-\overline{\phi_i},\mathbf{v}\cdot\nu_i\rangle_{\Gamma_i}=0,\quad\forall\mathbf{v}\in\mathbf{V}_{h,i}. \tag{2.14}$$

The projection operators have the following approximation properties:

$$\|\varphi-Q_h\varphi\|\leqslant C\|\varphi\|_t h^t,\quad 0\leqslant t\leqslant l+1, \tag{2.15}$$

$$\|\nabla\cdot(\mathbf{q}-\Pi_i\mathbf{q})\|_{\Omega_i}\leqslant C\|\nabla\cdot\mathbf{q}\|_{t,\Omega_i}h^t,\quad 0\leqslant t\leqslant l+1, \tag{2.16}$$

$$\|\mathbf{q}-\Pi_i\mathbf{q}\|_{\Omega_i}\leqslant C\|\mathbf{q}\|_{r,\Omega_i}h^r,\quad 1\leqslant r\leqslant k+1, \tag{2.17}$$

$$\|\phi-\overline{\phi_i}\|_{\Gamma_{ij}}\leqslant C\|\phi\|_{r,\Gamma_{ij}}h^r,\quad 0\leqslant r\leqslant k+1, \tag{2.18}$$

$$\|(\mathbf{q}-\Pi_i\mathbf{q})\cdot\nu_i\|_{\Gamma_{ij}}\leqslant C\|\mathbf{q}\|_{r,\Gamma_{ij}}h^r,\quad 0\leqslant r\leqslant k+1. \tag{2.19}$$

Bounds (2.18) and (2.19) are standard $L^2$-projection approximation results [13]; bounds (2.15)–(2.17) can be found in [11,28] for affine elements and in [30,5] for $h^2$-parallelograms.

In the analysis, we will also use the trace theorem

$$\|q\|_{r,\Gamma_{ij}}\leqslant C\|q\|_{r+1/2,\Omega_i},\quad r>0, \tag{2.20}$$

(see [20, Theorem 1.5.2.1]).

### 2.1. Mortar mixed finite element method

If the solution $(\mathbf{u},p)$ of (2.1)–(2.2) belongs to $H(\mathrm{div};\Omega)\times H^1(\Omega)$, it is easy to see that it satisfies, for $1\leqslant i\leqslant n$,

$$(K^{-1}\mathbf{u},\mathbf{v})_{\Omega_i}=(p,\nabla\cdot\mathbf{v})_{\Omega_i}-\langle p,\mathbf{v}\cdot\nu_i\rangle_{\Gamma_i}-\langle g,\mathbf{v}\cdot\nu_i\rangle_{\partial\Omega_i\setminus\Gamma_i},\quad\mathbf{v}\in\mathbf{V}_i, \tag{2.21}$$

$$(\nabla\cdot\mathbf{u},w)_{\Omega_i}=(f,w)_{\Omega_i},\quad w\in W_i. \tag{2.22}$$

Let $\mathscr{T}_{h,ij}$ be a shape-regular, quasi-uniform affine finite element partition of $\Gamma_{ij}$ and let $\mathscr{T}^{\Gamma,h}=\cup_{1\leqslant i<j\leqslant n}\mathscr{T}_{h,ij}$. Recall that $k$ is associated with the degree of the polynomials in $\mathbf{V}_h\cdot\nu$. Denote by $M_{h,ij}\subset L^2(\Gamma_{ij})$ the mortar finite element space on $\Gamma_{ij}$ containing at least either the continuous or discontinuous piecewise polynomials of degree $k+1$ on $\mathscr{T}_{h,ij}$. Let

$$M_h=\bigoplus_{1\leqslant i<j\leqslant n}M_{h,ij}$$

be the mortar finite element space on $\Gamma$. In the mortar mixed finite element approximation of (2.1)–(2.2) we seek $\mathbf{u}_h\in\mathbf{V}_h, p_h\in W_h$, and $\lambda_h\in M_h$ such that, for $1\leqslant i\leqslant n$,

$$(K^{-1}\mathbf{u}_h,\mathbf{v})_{\Omega_i}=(p_h,\nabla\cdot\mathbf{v})_{\Omega_i}-\langle\lambda_h,\mathbf{v}\cdot\nu_i\rangle_{\Gamma_i}-\langle g,\mathbf{v}\cdot\nu_i\rangle_{\partial\Omega_i\setminus\Gamma_i},\quad\mathbf{v}\in\mathbf{V}_{h,i}, \tag{2.23}$$

$$(\nabla\cdot\mathbf{u}_h,w)_{\Omega_i}=(f,w)_{\Omega_i},\quad w\in W_{h,i}, \tag{2.24}$$

$$\sum_{i=1}^{n}\langle\mathbf{u}_h\cdot\nu_i,\mu\rangle_{\Gamma_i}=0,\quad\mu\in M_h. \tag{2.25}$$

Note that we have a standard mixed finite element method within each block $\Omega_i$ and (2.24) enforces local conservation over each element. It is clear from (2.21) and (2.23) that $\lambda_h\in M_h$ is an approximation to the pressure $p$ on $\Gamma$. Eq. (2.25) enforces weak flux continuity across $\Gamma$ with respect to the mortar space $M_h$.

For the purpose of the analysis, it is convenient to eliminate $\lambda_h$ from the mortar mixed method (2.23)–(2.25) by restricting $\mathbf{V}_h$ to the space of weakly continuous velocities

$$\mathbf{V}_h^0=\left\{\mathbf{v}\in\mathbf{V}_h:\sum_{i=1}^{n}\langle\mathbf{v}_i\cdot\nu_i,\mu\rangle_{\Gamma_i}=0,\ \forall\mu\in M_h\right\}.$$

Problem (2.23)–(2.25) is equivalent to finding $\mathbf{u}_h\in\mathbf{V}_h^0$ and $p_h\in W_h$ such that

$$(K^{-1}\mathbf{u}_h,\mathbf{v}) = \sum_{i=1}^{n}(p_h,\nabla\cdot\mathbf{v})_{\Omega_i} - \langle g,\mathbf{v}\cdot\nu\rangle_{\partial\Omega}, \quad \mathbf{v}\in\mathbf{V}_h^0, \tag{2.26}$$

$$\sum_{i=1}^{n}(\nabla\cdot\mathbf{u}_h,w)_{\Omega_i} = (f,w), \quad w\in W_h. \tag{2.27}$$

Existence and uniqueness of a solution to (2.23)–(2.25) are shown in [34,1] along with optimal convergence and superconvergence for both pressure and velocity under the following condition.

**Assumption 2.1.** Assume that there exists a constant $C$ independent of $h$ such that

$$\|\mu\|_{\Gamma_{i,j}} \leqslant C(\|\overline{\mu_i}\|_{\Gamma_{i,j}} + \|\overline{\mu_j}\|_{\Gamma_{i,j}}), \quad \mu\in M_h, \quad 1\leqslant i<j\leqslant n. \tag{2.28}$$

**Remark 2.1.** The condition (2.28) imposes a limit on the number of mortar degrees of freedom and is easily satisfied in practice (see, e.g., [34,26]).

Assuming (2.28), the following superconvergence error estimates were shown in [1]:

$$\|\Pi\mathbf{u}-\mathbf{u}_h\| \leqslant C\sum_{i=1}^{n}(\|p\|_{k+5/2,\Omega_i} + \|\mathbf{u}\|_{k+3/2,\Omega_i})h^{k+3/2}, \tag{2.29}$$

$$\|Q_hp-p_h\| \leqslant C\sum_{i=1}^{n}(\|p\|_{r+2,\Omega_i} + \|\mathbf{u}\|_{r+1,\Omega_i} + \|\nabla\cdot\mathbf{u}\|_{r+1,\Omega_i})h^{r+2}, \quad r=\min(k,l). \tag{2.30}$$

Bound (2.29) was shown only for RT elements on rectangular grids. In the analysis, we will also use the optimal velocity error estimate [1]

$$\|\Pi\mathbf{u}-\mathbf{u}_h\| \leqslant C\sum_{i=1}^{n}(\|p\|_{k+2,\Omega_i} + \|\mathbf{u}\|_{k+1,\Omega_i})h^{k+1}. \tag{2.31}$$

The analysis in [1] is carried out for affine elements. It is easy to check that the estimates (2.30) and (2.31) also hold for $h^2$-parallelograms. The velocity superconvergence estimate (2.29) relies on the projection error orthogonality

$$(K^{-1}(\Pi_i\mathbf{u}-\mathbf{u}),\mathbf{v})_{\Omega_i} \leqslant Ch^{k+2}\|\mathbf{u}\|_{k+2,\Omega_i}\|\mathbf{v}\|_{\Omega_i}, \quad \mathbf{v}\in\mathbf{V}_{h,i}, \tag{2.32}$$

which was shown in [15, Theorem 3.1], for RT and BDFM spaces on rectangular elements in $\mathbb{R}^2$ and $\mathbb{R}^3$ and a diagonal tensor $K$. The results in [18] extend (2.32) to $h^2$-uniform quadrilaterals and full tensor coefficients. In particular, it is shown in [18, Theorem 5.1], that

$$(K^{-1}(\Pi_i\mathbf{u}-\mathbf{u}),\mathbf{v})_{\Omega_i} \leqslant Ch^{k+2}(\|\mathbf{u}\|_{k+2,\Omega_i}\|\mathbf{v}\|_{\Omega_i} + \|\mathbf{u}\|_{k+1,\Omega_i}\|\nabla\cdot\mathbf{v}\|_{\Omega_i}),$$
$$\forall\mathbf{v}\in\mathbf{V}_{h,i}, \quad \mathbf{v}\cdot\nu_i = 0 \text{ on } \partial\Omega_i, \tag{2.33}$$

and

$$(K^{-1}(\Pi_i\mathbf{u}-\mathbf{u}),\mathbf{v})_{\Omega_i} \leqslant Ch^{k+3/2}(\|\mathbf{u}\|_{k+3/2,\Omega_i}\|\mathbf{v}\|_{\Omega_i} + \|\mathbf{u}\|_{k+1,\Omega_i}\|\nabla\cdot\mathbf{v}\|_{\Omega_i}), \quad \forall \quad \mathbf{v}\in\mathbf{V}_{h,i}. \tag{2.34}$$

Using (2.34), it can be easily shown that (2.29) also holds for $h^2$-uniform quadrilateral grids and full tensor coefficients. In this paper we employ (2.33) to establish interior velocity superconvergence of order $\mathcal{O}(h^{k+2-\epsilon})$.

### 2.2. Non-mortar mixed finite element method

The non-mortar approach of [3] is based on using Robin type conditions for imposing continuity of pressures and fluxes across interfaces. To put the problem (2.1)–(2.2) in a multiblock form, choose a parameter $\alpha>0$ and write on each interface $\Gamma_{i,j}$

$$\alpha p_i - \mathbf{u}_i\cdot\nu_i = \alpha p_j + \mathbf{u}_j\cdot\nu_j, \quad \alpha p_j - \mathbf{u}_j\cdot\nu_j = \alpha p_i + \mathbf{u}_i\cdot\nu_i. \tag{2.35}$$

The Robin type interface conditions (2.35) imply

$$p_i = p_j, \quad \mathbf{u}_i\cdot\nu_i + \mathbf{u}_j\cdot\nu_j = 0,$$

i.e., both the pressure and the flux are continuous across $\Gamma_{i,j}$.

The non-mortar mixed finite element method is based on discretizing the subdomain variational equations (2.21)–(2.22) combined with a discrete weak imposition of the interface conditions (2.35). Let $\Lambda_{h,i}$ to be the hybrid mixed finite element Lagrange multiplier space on $\Gamma_i$ [4,19], i.e.,

$$\Lambda_{h,i} = \mathbf{V}_{h,i}\cdot\nu_i.$$

In the non-mortar mixed finite element approximation of (2.1)–(2.2), we seek $(\tilde{\mathbf{u}}_h,\tilde{p}_h)\in\mathbf{V}_h\times W_h$ and $\tilde{\lambda}_{h,i}\in\Lambda_{h,i}$ such that for $1\leqslant i\leqslant n$,

$$(K^{-1}\tilde{\mathbf{u}}_h,\mathbf{v})_{\Omega_i} = (\tilde{p}_h,\nabla\cdot\mathbf{v})_{\Omega_i} - \langle\tilde{\lambda}_{h,i},\mathbf{v}\cdot\nu_i\rangle_{\Gamma_i} - \langle g,\mathbf{v}\cdot\nu_i\rangle_{\partial\Omega_i\setminus\Gamma}, \quad \mathbf{v}\in\mathbf{V}_{h,i}, \tag{2.36}$$

$$(\nabla\cdot\tilde{\mathbf{u}}_h,w)_{\Omega_i} = (f,w)_{\Omega_i}, \quad w\in W_{h,i}, \tag{2.37}$$

$$\langle\alpha\tilde{\lambda}_{h,i}-\tilde{\mathbf{u}}_{h,i}\cdot\nu_i,\mu_i\rangle_{\Gamma_i} = \sum_{j=1}^{n}\langle\alpha\tilde{\lambda}_{h,j}+\tilde{\mathbf{u}}_{h,j}\cdot\nu_j,\mu_i\rangle_{\Gamma_{i,j}}, \quad \mu_i\in\Lambda_{h,i}. \tag{2.38}$$

We can replace (2.38) with the condition that for $1\leqslant i\leqslant n$

$$\sum_{j=1}^{n}\langle\alpha(\tilde{\lambda}_{h,i}-\tilde{\lambda}_{h,j}),\mu_i\rangle_{\Gamma_{i,j}} = \sum_{j=1}^{n}\langle\tilde{\mathbf{u}}_{h,i}\cdot\nu_i+\tilde{\mathbf{u}}_{h,j}\cdot\nu_j,\mu_i\rangle_{\Gamma_{i,j}}, \quad \mu_i\in\Lambda_{h,i}. \tag{2.39}$$

Existence and uniqueness of a solution to (2.36)–(2.38) are shown in [3] along with optimal convergence for both pressure and velocity:

$$\|p-\tilde{p}_h\| + \|\mathbf{u}-\tilde{\mathbf{u}}_h\| + \left(\alpha\sum_{i,j}\|\tilde{\lambda}_{h,i}-\tilde{\lambda}_{h,j}\|^2_{\Gamma_{i,j}}\right)^{1/2} + \left(\frac{1}{\alpha}\sum_{i,j}\|\tilde{\mathbf{u}}_{h,i}\cdot\nu_i+\tilde{\mathbf{u}}_{h,j}\cdot\nu_j\|^2_{\Gamma_{i,j}}\right)^{1/2} \leqslant C\sum_{i=1}^{n}(\|p\|_{r+3/2,\Omega_i} + \|\mathbf{u}\|_{r+3/2,\Omega_i})h^{r+1}, \quad r=\min(k,l), \tag{2.40}$$

$$\left\{\sum_{i=1}^{n}\|\nabla\cdot(\mathbf{u}-\tilde{\mathbf{u}}_{h,i})\|^2_{\Omega_i}\right\}^{1/2} \leqslant C\sum_{i=1}^{n}\|\nabla\cdot\mathbf{u}\|_{l+1,\Omega_i}h^{l+1}. \tag{2.41}$$

## 3. Interior estimates for the mortar mixed finite element method

In this section, we establish interior superconvergence for the velocity in the mortar mixed finite element method. The results in the section are valid in the following cases.

(A1) The mixed finite element spaces are either RT or BDFM. The grids are either $h^2$-uniform quadrilateral in $\mathbb{R}^2$ or rectangular in $\mathbb{R}^3$. In the latter case, $K$ is assumed to be a diagonal tensor.

The interior error analysis is based on multiplying the test functions by appropriate smooth cutoff functions. We will make use of the following lemma.

**Lemma 3.1.** *If $\phi\in H^1(\Omega)$ and $\mathbf{v}\in\mathbf{V}_h$, then there exists a constant $C$ independent of $h$ such that*
$\|(I-\Pi)(\phi\mathbf{v})\| \leqslant C\|\mathbf{v}\|\|\phi\|_1 h.$

**Proof.** For any $\mathbf{v}\in\mathbf{V}_h$, consider the functional

$$l_{\mathbf{v}}(\phi) = \phi\mathbf{v} - \Pi(\phi\mathbf{v}).$$

Since $l_{\mathbf{v}}(\phi) = 0$ for all constant functions $\phi$, the statement of the lemma follows from an application of the Bramble–Hilbert lemma [13]. □

Let $\Omega_i'$ be compactly contained in $\Omega_i, i = 1, \ldots, n$ and let $\Omega' = \cup_{i=1}^n \Omega_i'$.

We prove the following interior velocity error estimates for the mortar mixed finite element method.

**Theorem 3.1.** *Assume (A1) and that (1.5) holds. Then, for any $\varepsilon > 0$, there exists a constant $C_\varepsilon$ dependent on the distance between $\Omega'$ and $\Gamma$, but independent of $h$ such that*

$$\|\Pi\mathbf{u} - \mathbf{u}_h\|_{\Omega'} \leqslant C_\varepsilon \sum_{i=1}^n (\|p\|_{k+2,\Omega_i} + \|\mathbf{u}\|_{k+2,\Omega_i} + \|\nabla\cdot\mathbf{u}\|_{k+1,\Omega_i}) h^{k+2-\varepsilon}.$$

**Proof.** Key ingredients in the proof of the theorem are the optimal velocity convergence (2.31), the projection error orthogonality (2.33), and the superconvergence for pressure (2.30).

The error equations for the mortar mixed finite element method are obtained by subtracting (2.23)–(2.24) from (2.21)–(2.22):

$$(K^{-1}(\mathbf{u} - \mathbf{u}_h), \mathbf{v}) = \sum_{i=1}^n ((p - p_h, \nabla\cdot\mathbf{v})_{\Omega_i} - \langle p, \mathbf{v}\cdot\nu_i\rangle_{\Gamma_i}), \quad \mathbf{v} \in \mathbf{V}_h^0, \tag{3.1}$$

$$\sum_{i=1}^n (\nabla\cdot(\mathbf{u} - \mathbf{u}_h), w)_{\Omega_i} = 0, \quad w \in W_h. \tag{3.2}$$

Note that (3.2), (2.9), and either (2.11) or (2.12) imply that

$$\nabla\cdot(\Pi\mathbf{u} - \mathbf{u}_h) = 0. \tag{3.3}$$

For $i = 1, \ldots, n$, consider subdomain sequences $\Omega_i^j$, $j = 1, 2, \ldots$ such that

$$\Omega_i' \subset\subset \Omega_i^{j+1} \subset\subset \Omega_i^j \subset\subset \Omega_i.$$

Let $\Omega^j = \cup_{i=1}^n \Omega_i^j$. Let $\phi_{j+1} \in C_0^\infty(\Omega^j)$ be a cutoff function, $\phi_{j+1} \geqslant 0, \phi_{j+1} \equiv 1$ on $\Omega^{j+1}$, and $\phi_{j+1} \leqslant 1$ on $\Omega^j$. The constants that appear below may depend on $\|\phi_{j+1}\|_{1,\infty,\Omega^j}$. Note that, since $\phi_j \equiv 1$ on $\Omega^j$,

$$\|\mathbf{v}\|_{\Omega^j} = \|\phi_j^{1/2}\mathbf{v}\|_{\Omega^j} \leqslant \|\phi_j^{1/2}\mathbf{v}\|_{\Omega^{j-1}},$$

which will be used repeatedly in our argument.

We have, using (3.1) with $\mathbf{v} = \Pi\phi_{j+1}(\Pi\mathbf{u} - \mathbf{u}_h)$,

$$\begin{aligned}
c\|\phi_{j+1}^{1/2}(\Pi\mathbf{u} - \mathbf{u}_h)\|_{\Omega^j}^2 &\leqslant (K^{-1}(\Pi\mathbf{u} - \mathbf{u}_h), \phi_{j+1}(\Pi\mathbf{u} - \mathbf{u}_h))_{\Omega^j} \\
&= (K^{-1}(\Pi\mathbf{u} - \mathbf{u}_h), (I - \Pi)(\phi_{j+1}(\Pi\mathbf{u} - \mathbf{u}_h)))_{\Omega^j} \\
&\quad + (K^{-1}(\Pi\mathbf{u} - \mathbf{u}_h), \Pi\phi_{j+1}(\Pi\mathbf{u} - \mathbf{u}_h))_{\Omega^j} \\
&= (K^{-1}(\Pi\mathbf{u} - \mathbf{u}_h), (I - \Pi)(\phi_{j+1}(\Pi\mathbf{u} - \mathbf{u}_h)))_{\Omega^j} \\
&\quad + (K^{-1}(\Pi\mathbf{u} - \mathbf{u}), \Pi\phi_{j+1}(\Pi\mathbf{u} - \mathbf{u}_h))_{\Omega^j} \\
&\quad + \sum_{i=1}^n (p - p_h, \nabla\cdot(\Pi\phi_{j+1}(\Pi\mathbf{u} - \mathbf{u}_h)))_{\Omega_i^j} \\
&\leqslant C\|\Pi\mathbf{u} - \mathbf{u}_h\|_{\Omega^j}\|(I - \Pi)(\phi_{j+1}(\Pi\mathbf{u} - \mathbf{u}_h))\|_{\Omega^j} \\
&\quad + Ch^{k+2}\|\mathbf{u}\|_{k+2,\Omega^j}\|\Pi\phi_{j+1}(\Pi\mathbf{u} - \mathbf{u}_h)\|_{\Omega^j} \\
&\quad + Ch^{k+2}\|\mathbf{u}\|_{k+1,\Omega^j}\|\nabla\cdot\Pi\phi_{j+1}(\Pi\mathbf{u} - \mathbf{u}_h)\|_{\Omega^j} \\
&\quad + (p - p_h, \nabla\cdot\Pi\phi_{j+1}(\Pi\mathbf{u} - \mathbf{u}_h))_{\Omega^j},
\end{aligned} \tag{3.4}$$

where we have used either (2.32) (for rectangular grids in $\mathbb{R}^3$) or (2.33) (for $h^2$-uniform quadrilateral grids) in the last inequality. Using (2.31) and Lemma 3.1, the first term on the right can be estimated as

$$\begin{aligned}
&\|\Pi\mathbf{u} - \mathbf{u}_h\|_{\Omega^j}\|(I - \Pi)(\phi_{j+1}(\Pi\mathbf{u} - \mathbf{u}_h))\|_{\Omega^j} \\
&\quad \leqslant C\sum_{i=1}^n (\|p\|_{k+2,\Omega_i} + \|\mathbf{u}\|_{k+1,\Omega_i}) h^{k+1}\|\Pi\mathbf{u} - \mathbf{u}_h\|_{\Omega^j}\|\phi_{j+1}\|_{1,\Omega^j}\ h \\
&\quad \leqslant C\sum_{i=1}^n (\|p\|_{k+2,\Omega_i} + \|\mathbf{u}\|_{k+1,\Omega_i}) h^{k+2}\|\phi_j^{1/2}(\Pi\mathbf{u} - \mathbf{u}_h)\|_{\Omega^{j-1}}.
\end{aligned} \tag{3.5}$$

For the second term on the right in (3.4) we have

$$\begin{aligned}
\|\Pi\phi_{j+1}(\Pi\mathbf{u} - \mathbf{u}_h)\|_{\Omega^j} &\leqslant \|(I - \Pi)\phi_{j+1}(\Pi\mathbf{u} - \mathbf{u}_h)\|_{\Omega^j} \\
&\quad + \|\phi_{j+1}(\Pi\mathbf{u} - \mathbf{u}_h)\|_{\Omega^j} \\
&\leqslant Ch\|\Pi\mathbf{u} - \mathbf{u}_h\|_{\Omega^j}\|\phi_{j+1}\|_{1,\Omega^j} \\
&\quad + \|\phi_{j+1}\|_{\infty,\Omega^j}\|\Pi\mathbf{u} - \mathbf{u}_h\|_{\Omega^j} \\
&\leqslant C\|\phi_j^{1/2}(\Pi\mathbf{u} - \mathbf{u}_h)\|_{\Omega^{j-1}},
\end{aligned} \tag{3.6}$$

using Lemma 3.1 for the second inequality. For the third term on the right in (3.4), using (2.16) and (3.3), we have

$$\begin{aligned}
\|\nabla\cdot\Pi\phi_{j+1}(\Pi\mathbf{u} - \mathbf{u}_h)\|_{\Omega^j} &\leqslant C\|\nabla\cdot\phi_{j+1}(\Pi\mathbf{u} - \mathbf{u}_h)\|_{\Omega^j} \\
&= C\|\nabla\phi_{j+1}\cdot(\Pi\mathbf{u} - \mathbf{u}_h)\|_{\Omega^j} \\
&\leqslant C\|\phi_{j+1}\|_{1,\infty,\Omega^j}\|\Pi\mathbf{u} - \mathbf{u}_h\|_{\Omega^j} \\
&\leqslant C\|\phi_j^{1/2}(\Pi\mathbf{u} - \mathbf{u}_h)\|_{\Omega^{j-1}}.
\end{aligned} \tag{3.7}$$

Similarly, using (2.13), (2.9) and (3.3), the last term on the right in (3.4) can be bounded as

$$\begin{aligned}
(p - p_h, \nabla\cdot\Pi(\phi_{j+1}(\Pi\mathbf{u} - \mathbf{u}_h)))_{\Omega^j} &= (Q_hp - p_h, \nabla\cdot\Pi(\phi_{j+1}(\Pi\mathbf{u} - \mathbf{u}_h)))_{\Omega^j} \\
&= (Q_hp - p_h, \nabla\phi_{j+1}\cdot(\Pi\mathbf{u} - \mathbf{u}_h))_{\Omega^j} \\
&\leqslant C\|Q_hp - p_h\|_{\Omega^j}\|\phi_j^{1/2}(\Pi\mathbf{u} - \mathbf{u}_h)\|_{\Omega^{j-1}} \\
&\leqslant C\sum_{i=1}^n (\|p\|_{k+2,\Omega_i} + \|\mathbf{u}\|_{k+1,\Omega_i} \\
&\quad + \|\nabla\cdot\mathbf{u}\|_{k+1,\Omega_i}) h^{k+2}\|\phi_j^{1/2}(\Pi\mathbf{u} - \mathbf{u}_h)\|_{\Omega^{j-1}},
\end{aligned} \tag{3.8}$$

using (2.30) in the last inequality.

Combining (3.4)–(3.8), we get

$$\begin{aligned}
\|\phi_{j+1}^{1/2}(\Pi\mathbf{u} - \mathbf{u}_h)\|_{\Omega^j} &\leqslant Ch^{\frac{k+2}{2}}\|\phi_j^{1/2}(\Pi\mathbf{u} - \mathbf{u}_h)\|_{\Omega^{j-1}}^{1/2} \\
&\quad \times \left(\sum_{i=1}^n (\|p\|_{k+2,\Omega_i} + \|\mathbf{u}\|_{k+2,\Omega_i} + \|\nabla\cdot\mathbf{u}\|_{k+1,\Omega_i})\right)^{1/2} \\
&\equiv Ch^{\frac{k+2}{2}}\|\phi_j^{1/2}(\Pi\mathbf{u} - \mathbf{u}_h)\|_{\Omega^{j-1}}^{1/2} A^{1/2}.
\end{aligned} \tag{3.9}$$

Replacing $j + 1$ with $j$ in (3.9), we obtain

$$\|\phi_j^{1/2}(\Pi\mathbf{u} - \mathbf{u}_h)\|_{\Omega^{j-1}}^{1/2} \leqslant Ch^{\frac{k+2}{4}}\|\phi_{j-1}^{1/2}(\Pi\mathbf{u} - \mathbf{u}_h)\|_{\Omega^{j-2}}^{1/4} A^{1/4}. \tag{3.10}$$

Multiplying (3.9) and (3.10) recurrently leads to

$$\|\phi_{j+1}^{1/2}(\Pi\mathbf{u} - \mathbf{u}_h)\|_{\Omega^j} \leqslant Ch^{(k+2)\left(\frac{1}{2}+\frac{1}{4}+\cdots\right)} A^{\frac{1}{2}+\frac{1}{4}+\cdots} \leqslant Ch^{k+2-\varepsilon}A,$$

where we take enough terms so that $\frac{1}{2} + \frac{1}{4} + \cdots \geqslant 1 - \frac{\varepsilon}{k+2}$. □

## 4. Interior estimates for the non-mortar mixed finite element method

Similarly to the case of mortar mixed finite element method, subtracting Eqs. (2.36)–(2.37) from (2.21)–(2.22) and using properties of the projections, we get the error equations for the non-mortar mixed finite element method

$$\begin{aligned}
&(K^{-1}(\mathbf{u} - \tilde{\mathbf{u}}_h), \mathbf{v})_{\Omega_i} = (Q_hp - \tilde{p}_h, \nabla\cdot\mathbf{v})_{\Omega_i} - \langle p_i - \tilde{\lambda}_{h,i}, \mathbf{v}\cdot\nu_i\rangle_{\Gamma_i}, \\
&\quad \mathbf{v} \in \mathbf{V}_{h,i},
\end{aligned} \tag{4.1}$$

$$(\nabla\cdot(\mathbf{u}-\tilde{\mathbf{u}}_h),w)_{\Omega_i}=0,\quad w\in W_{h,i}. \tag{4.2}$$

Here for clarity of notation we have denoted the trace of $p$ on $\Gamma_i$ by $p_i$, although, by the assumption $p\in H^1(\Omega)$, $p$ has a single-valued trace on $\Gamma$.

One of the key ingredients in the proof of Theorem 3.1, namely superconvergence for pressure, is missing in the analysis of [3]. Using a duality argument, we prove the following pressure superconvergence theorem.

**Theorem 4.1.** *Assume (1.5) and that any of the usual mixed spaces on affine elements or RT or BDFM on $h^2$-parallelograms are used. For the pressure $\tilde{p}_h$ of the non-mortar mixed method (2.36)–(2.38), there exists a positive constant C, independent of h, such that*

$$\|Q_hp-\tilde{p}_h\|\leqslant C\sum_{i=1}^{n}(\|p\|_{r+3/2,\Omega_i}+\|\mathbf{u}\|_{r+3/2,\Omega_i}+\|\nabla\cdot\mathbf{u}\|_{r+1,\Omega_i})h^{r+3/2},$$

$r=\min(k,l)$.

**Proof.** Let $\xi\in H^2(\Omega)$ be the solution of the auxiliary problem

$$-\nabla\cdot K\nabla\xi=Q_hp-\tilde{p}_h\quad\text{in }\Omega,$$
$$\xi=0\quad\text{on }\partial\Omega,$$

and note that by (1.5)

$$\|\xi\|_2\leqslant C\|Q_hp-\tilde{p}_h\|. \tag{4.3}$$

Let $\zeta=-K\nabla\xi$. Taking $\mathbf{v}=\Pi_i\zeta\in\mathbf{V}_{h,i}$ in (4.1) and using (2.9), we have

$$\begin{aligned}\|Q_hp-\tilde{p}_h\|_{\Omega_i}^2&=(Q_hp-\tilde{p}_h,\nabla\cdot\Pi_i\zeta)_{\Omega_i}\\&=(K^{-1}(\mathbf{u}-\tilde{\mathbf{u}}_h),\Pi_i\zeta-\zeta)_{\Omega_i}-(\mathbf{u}-\tilde{\mathbf{u}}_h,\nabla\xi)_{\Omega_i}\\&\quad+\langle p_i-\tilde{\lambda}_{h,i},\Pi_i\zeta\cdot\boldsymbol{\nu}_i\rangle_{\Gamma_i}.\end{aligned}$$

Sum over $i$ and use (2.14) to get

$$\begin{aligned}\|Q_hp-\tilde{p}_h\|^2&=\sum_{i=1}^{n}(K^{-1}(\mathbf{u}-\tilde{\mathbf{u}}_h),\Pi_i\zeta-\zeta)_{\Omega_i}-\sum_{i=1}^{n}(\mathbf{u}-\tilde{\mathbf{u}}_h,\nabla\xi)_{\Omega_i}\\&\quad+\sum_{i=1}^{n}\langle\overline{p}_i-\tilde{\lambda}_{h,i},\Pi_i\zeta\cdot\boldsymbol{\nu}_i\rangle_{\Gamma_i}\\&=\sum_{i=1}^{n}(K^{-1}(\mathbf{u}-\tilde{\mathbf{u}}_h),\Pi_i\zeta-\zeta)_{\Omega_i}\\&\quad+\sum_{i=1}^{n}(\nabla\cdot(\mathbf{u}-\tilde{\mathbf{u}}_h),\xi-Q_h\xi)_{\Omega_i}-\sum_{i=1}^{n}\langle(\mathbf{u}-\tilde{\mathbf{u}}_{h,i})\cdot\boldsymbol{\nu}_i,\xi\rangle_{\Gamma_i}\\&\quad+\sum_{i=1}^{n}\langle\overline{p}_i-\tilde{\lambda}_{h,i},\zeta_i\cdot\boldsymbol{\nu}_i\rangle_{\Gamma_i},\end{aligned} \tag{4.4}$$

where we integrated by parts the second term and used (4.2) and (2.10). The first two terms on the right in (4.4) are easy to handle. Using (4.3) and the approximation properties (2.17), (2.15), we get

$$\begin{aligned}&\sum_{i=1}^{n}(K^{-1}(\mathbf{u}-\tilde{\mathbf{u}}_h),\Pi_i\zeta-\zeta)_{\Omega_i}+\sum_{i=1}^{n}(\nabla\cdot(\mathbf{u}-\tilde{\mathbf{u}}_h),\xi-Q_h\xi)_{\Omega_i}\\&\quad\leqslant C\left(\|\mathbf{u}-\tilde{\mathbf{u}}_h\|+\sum_{i=1}^{n}\|\nabla\cdot(\mathbf{u}-\tilde{\mathbf{u}}_h)\|_{\Omega_i}\right)h\|Q_hp-\tilde{p}_h\|.\end{aligned} \tag{4.5}$$

Using the continuity of $\xi$ and $\mathbf{u}$, we rearrange the third term in (4.4) to obtain

$$\begin{aligned}-\sum_{i=1}^{n}\langle(\mathbf{u}-\tilde{\mathbf{u}}_{h,i})\cdot\boldsymbol{\nu}_i,\xi\rangle_{\Gamma_i}&=-\frac{1}{2}\sum_{i,j}\langle(\mathbf{u}-\tilde{\mathbf{u}}_{h,i})\cdot\boldsymbol{\nu}_i+(\mathbf{u}-\tilde{\mathbf{u}}_{h,j})\cdot\boldsymbol{\nu}_j,\xi\rangle_{\Gamma_{ij}}\\&=\frac{1}{2}\sum_{i,j}\langle\tilde{\mathbf{u}}_{h,i}\cdot\boldsymbol{\nu}_i+\tilde{\mathbf{u}}_{h,j}\cdot\boldsymbol{\nu}_j,\overline{\xi}_i\rangle_{\Gamma_{ij}}\\&\quad+\frac{1}{2}\sum_{i,j}\langle\tilde{\mathbf{u}}_{h,i}\cdot\boldsymbol{\nu}_i+\tilde{\mathbf{u}}_{h,j}\cdot\boldsymbol{\nu}_j,\xi-\overline{\xi}_i\rangle_{\Gamma_{ij}}.\end{aligned} \tag{4.6}$$

Bounding the second term on the right in (4.6) is straightforward: bounds (2.18), (2.20) and (4.3) give

$$\begin{aligned}\sum_{i,j}\langle\tilde{\mathbf{u}}_{h,i}\cdot\boldsymbol{\nu}_i+\tilde{\mathbf{u}}_{h,j}\cdot\boldsymbol{\nu}_j,\xi-\overline{\xi}_i\rangle_{\Gamma_{ij}}&\leqslant\left(\sum_{i,j}\|\tilde{\mathbf{u}}_{h,i}\cdot\boldsymbol{\nu}_i+\tilde{\mathbf{u}}_{h,j}\cdot\boldsymbol{\nu}_j\|_{\Gamma_{ij}}^2\right)^{1/2}\\&\quad\times\left(\sum_{i,j}\|\xi-\overline{\xi}_i\|_{\Gamma_{ij}}^2\right)^{1/2}\\&\leqslant C\left(\sum_{i,j}\|\tilde{\mathbf{u}}_{h,i}\cdot\boldsymbol{\nu}_i+\tilde{\mathbf{u}}_{h,j}\cdot\boldsymbol{\nu}_j\|_{\Gamma_{ij}}^2\right)^{1/2}\\&\quad\times h\left(\sum_{i}\|\xi\|_{3/2,\Omega_i}^2\right)^{1/2}\\&\leqslant C\left(\sum_{i,j}\|\tilde{\mathbf{u}}_{h,i}\cdot\boldsymbol{\nu}_i+\tilde{\mathbf{u}}_{h,j}\cdot\boldsymbol{\nu}_j\|_{\Gamma_{ij}}^2\right)^{1/2}\\&\quad\times h\|Q_hp-\tilde{p}_h\|.\end{aligned} \tag{4.7}$$

To handle the first term on the right in (4.6), we take $\mu_i=\frac{1}{2}\overline{\xi}_i$ in (2.39), sum over $i$ and rearrange to get

$$\begin{aligned}\frac{1}{2}\sum_{i,j}\langle\tilde{\mathbf{u}}_{h,i}\cdot\boldsymbol{\nu}_i+\tilde{\mathbf{u}}_{h,j}\cdot\boldsymbol{\nu}_j,\overline{\xi}_i\rangle_{\Gamma_{ij}}&=\frac{1}{2}\sum_{i,j}\langle\alpha(\tilde{\lambda}_{h,i}-\tilde{\lambda}_{h,j}),\overline{\xi}_i\rangle_{\Gamma_{ij}}\\&=\frac{1}{2}\sum_{i<j}\langle\alpha(\tilde{\lambda}_{h,i}-\tilde{\lambda}_{h,j}),\overline{\xi}_i-\overline{\xi}_j\rangle_{\Gamma_{ij}}\\&=\frac{1}{2}\sum_{i<j}\langle\alpha(\tilde{\lambda}_{h,i}-\tilde{\lambda}_{h,j}),(\overline{\xi}_i-\xi)+(\xi-\overline{\xi}_j)\rangle_{\Gamma_{ij}}\\&\leqslant\frac{1}{2}\sum_{i<j}\alpha\|\tilde{\lambda}_{h,i}-\tilde{\lambda}_{h,j}\|_{\Gamma_{ij}}\\&\quad\times(\|\xi_i-\overline{\xi}_i\|_{\Gamma_{ij}}+\|\xi_j-\overline{\xi}_j\|_{\Gamma_{ij}})\\&\leqslant C\sum_{i<j}\alpha\|\tilde{\lambda}_{h,i}-\tilde{\lambda}_{h,j}\|_{\Gamma_{ij}}\\&\quad\times h(\|\xi\|_{3/2,\Omega_i}+\|\xi\|_{3/2,\Omega_j})\\&\leqslant C\sum_{i<j}\alpha\|\tilde{\lambda}_{h,i}-\tilde{\lambda}_{h,j}\|_{\Gamma_{ij}}h\|Q_hp-\tilde{p}_h\|,\end{aligned} \tag{4.8}$$

where we used (2.18), (2.20) and (4.3) in the last inequality. It remains to bound the last term in (4.4). Using the continuity of $\zeta\cdot\boldsymbol{\nu}$ and $p$, and rearranging terms, we obtain

$$\begin{aligned}\sum_{i=1}^{n}\langle\overline{p}_i-\tilde{\lambda}_{h,i},\zeta_i\cdot\boldsymbol{\nu}_i\rangle_{\Gamma_i}&=\frac{1}{2}\sum_{i,j}\langle\overline{p}_i-\tilde{\lambda}_{h,i}-\overline{p}_j+\tilde{\lambda}_{h,j},\zeta_i\cdot\boldsymbol{\nu}_i\rangle_{\Gamma_{ij}}\\&=\frac{1}{2}\sum_{i,j}\langle\overline{p}_i-\overline{p}_j-\tilde{\lambda}_{h,i}+\tilde{\lambda}_{h,j},(\zeta_i-\Pi_i\zeta_i)\cdot\boldsymbol{\nu}_i\rangle_{\Gamma_{ij}}\\&\quad-\frac{1}{2}\sum_{i,j}\langle\tilde{\lambda}_{h,i}-\tilde{\lambda}_{h,j},\Pi_i\zeta_i\cdot\boldsymbol{\nu}_i\rangle_{\Gamma_{ij}}\\&\quad+\frac{1}{2}\sum_{i,j}\langle\overline{p}_i-\overline{p}_j,\Pi_i\zeta_i\cdot\boldsymbol{\nu}_i\rangle_{\Gamma_{ij}}.\end{aligned} \tag{4.9}$$

The first term in (4.9) can be bounded using (2.18)–(2.20) and (4.3),

$$\begin{aligned}&\langle\overline{p}_i-\overline{p}_j-\tilde{\lambda}_{h,i}+\tilde{\lambda}_{h,j},(\zeta_i-\Pi_i\zeta_i)\cdot\boldsymbol{\nu}_i\rangle_{\Gamma_{ij}}\\&\quad\leqslant(\|p_i-\overline{p}_i\|_{\Gamma_{ij}}+\|p_j-\overline{p}_j\|_{\Gamma_{ij}}+\|\tilde{\lambda}_{h,i}-\tilde{\lambda}_{h,j}\|_{\Gamma_{ij}})\|(\zeta_i-\Pi_i\zeta_i)\cdot\boldsymbol{\nu}_i\|_{\Gamma_{ij}}\\&\quad\leqslant C\left(h^{k+1}\|p_i\|_{k+3/2,\Omega_i}+h^{k+1}\|p_j\|_{k+3/2,\Omega_j}+\|\tilde{\lambda}_{h,i}-\tilde{\lambda}_{h,j}\|_{\Gamma_{ij}}\right)h^{1/2}\|\boldsymbol{\zeta}\|_{1,\Omega_i}\\&\quad\leqslant C\left(h^{k+1}\|p_i\|_{k+3/2,\Omega_i}+h^{k+1}\|p_j\|_{k+3/2,\Omega_j}+\|\tilde{\lambda}_{h,i}-\tilde{\lambda}_{h,j}\|_{\Gamma_{ij}}\right)\\&\qquad\times h^{1/2}\|Q_hp-\tilde{p}_h\|.\end{aligned} \tag{4.10}$$

To handle the second term in (4.9), take $\mu_i = \frac{1}{2\alpha}\Pi_i\zeta_i \cdot \nu_i$ in (2.39), sum over $i$, combine the two terms on $\Gamma_{i,j}$ and use the continuity of $\zeta \cdot \nu$ to obtain

$$
\begin{aligned}
&-\frac{1}{2}\sum_{i,j}\langle\tilde{\lambda}_{h,i}-\tilde{\lambda}_{h,j},\Pi_i\zeta_i\cdot\nu_i\rangle_{\Gamma_{i,j}}\\
&=-\frac{1}{2\alpha}\sum_{i,j}\langle\tilde{\mathbf{u}}_{h,i}\cdot\nu_i+\tilde{\mathbf{u}}_{h,j}\cdot\nu_j,\Pi_i\zeta_i\cdot\nu_i\rangle_{\Gamma_{i,j}}\\
&=-\frac{1}{2\alpha}\sum_{i<j}\langle\tilde{\mathbf{u}}_{h,i}\cdot\nu_i+\tilde{\mathbf{u}}_{h,j}\cdot\nu_j,\Pi_i\zeta_i\cdot\nu_i+\Pi_j\zeta_j\cdot\nu_j\rangle_{\Gamma_{i,j}}\\
&=\frac{1}{2\alpha}\sum_{i<j}\langle(\tilde{\mathbf{u}}_{h,i}\cdot\nu_i+\tilde{\mathbf{u}}_{h,j}\cdot\nu_j),(\zeta_i-\Pi_i\zeta_i)\cdot\nu_i+(\zeta_j-\Pi_j\zeta_j)\cdot\nu_j\rangle_{\Gamma_{i,j}}\\
&\leqslant\frac{1}{2\alpha}\sum_{i<j}\|\tilde{\mathbf{u}}_{h,i}\cdot\nu_i+\tilde{\mathbf{u}}_{h,j}\cdot\nu_j\|_{\Gamma_{i,j}}(\|(\zeta_i-\Pi_i\zeta_i)\cdot\nu_i\|_{\Gamma_{i,j}}\\
&\quad+\|(\zeta_j-\Pi_j\zeta_j)\cdot\nu_j\|_{\Gamma_{i,j}})\\
&\leqslant C\sum_{i<j}\frac{1}{2\alpha}\|\tilde{\mathbf{u}}_{h,i}\cdot\nu_i+\tilde{\mathbf{u}}_{h,j}\cdot\nu_j\|_{\Gamma_{i,j}}h^{1/2}\|Q_hp-\tilde{p}_h\|,
\end{aligned}
\tag{4.11}
$$

where we used (2.19), (2.20) and (4.3) in the last inequality. Finally, for the last term in (4.9), applying (2.14) and using the continuity of $p$ and $\zeta \cdot \nu$, we get

$$
\begin{aligned}
&\frac{1}{2}\sum_{i,j}\langle\overline{p_i}-\overline{p_j},\Pi_i\zeta_i\cdot\nu_i\rangle_{\Gamma_{i,j}}\\
&=\frac{1}{2}\sum_{i,j}\langle p_i-\overline{p_j},\Pi_i\zeta_i\cdot\nu_i\rangle_{\Gamma_{i,j}}\\
&=\frac{1}{2}\sum_{i,j}\langle p_j-\overline{p_j},\Pi_i\zeta_i\cdot\nu_i+\Pi_j\zeta_j\cdot\nu_j\rangle_{\Gamma_{i,j}}\\
&=\frac{1}{2}\sum_{i,j}\langle p_j-\overline{p_j},(\Pi_i\zeta_i-\zeta_i)\cdot\nu_i+(\Pi_j\zeta_j-\zeta_j)\cdot\nu_j\rangle_{\Gamma_{i,j}}\\
&\leqslant\frac{1}{2}\sum_{i,j}\|p_j-\overline{p_j}\|_{\Gamma_{i,j}}(\|(\zeta_i-\Pi_i\zeta_i)\cdot\nu_i\|_{\Gamma_{i,j}}+\|(\zeta_j-\Pi_j\zeta_j)\cdot\nu_j\|_{\Gamma_{i,j}})\\
&\leqslant C\sum_{i,j}h^{k+1}\|p\|_{k+3/2,\Omega_j}h^{1/2}\|Q_hp-\tilde{p}_h\|,
\end{aligned}
\tag{4.12}
$$

using (2.18)–(2.20) and (4.3) in the last inequality. A combination of (4.4)–(4.12) and the use of (2.40) and (2.41) completes the proof. □

We are now ready to establish an interior velocity error estimate for the non-mortar mixed finite element method.

**Theorem 4.2.** *Assume (A1) and that (1.5) holds. Then, for any $\varepsilon > 0$, there exist a constant $C_\varepsilon$ dependent on the distance between $\Omega'$ and $\Gamma$, but independent of $h$ such that*

$$
\begin{aligned}
\|\Pi\mathbf{u}-\tilde{\mathbf{u}}_h\|_{\Omega'}\leqslant C_\varepsilon\sum_{i=1}^{n}(&\|p\|_{k+3/2,\Omega_i}+\|\mathbf{u}\|_{k+3/2,\Omega_i}+\|\nabla\\
&\cdot\mathbf{u}\|_{k+1,\Omega_i})h^{k+3/2-\varepsilon}.
\end{aligned}
$$

The proof is similar to the proof of Theorem 3.1 and it is omitted.

## 5. Numerical results

We present several numerical tests using the lowest order RT spaces ($k = 0$) on rectangles and quadrilaterals to confirm the theoretical results of Sections 3 and 4. The first four examples are on the unit square and the fifth one is on the unit cube. The last two examples test quadrilateral grids on irregular domains obtained by a mapping of the unit square.

The domain is divided into four (eight for Example 5.5) subdomains with interfaces along the $x = 1/2$ and $y = 1/2$ (and $z = 1/2$ for Example 5.5) lines. Recall that optimal convergence for the solution to (2.23)–(2.25) holds under the assumption that $M_h$ contains at least piecewise polynomials of degree $k+1$ [1], which in this case means piecewise linear functions. We test three types of methods on non-matching interfaces: 1 (continuous piecewise linear mortars), 2 (discontinuous piecewise linear mortars), and 3 (Robin type interface conditions – non-mortar mixed finite element method). In the fourth example we also test matching grids (denoted by mortar 0). In the numerical experiments we report the rates of convergence of the numerical solution (pressure and velocity) to the true solution. We compute the velocity error in the discrete $L^2$-norm

$$
|||\mathbf{v}|||^2=\sum_{E\in\mathcal{T}_h}\sum_{e\in\partial E}|E|(\mathbf{v}\cdot\nu_e)^2(m_e),
$$

where $m_e$ is the midpoint of edge (face) $e$. It is easy to see that

$$
c_1\|\mathbf{v}\|\leqslant|||\mathbf{v}|||\leqslant c_2\|\mathbf{v}\|\quad\forall\quad\mathbf{v}\in\mathbf{V}_h
$$

and

$$
|||\mathbf{u}-\Pi\mathbf{u}|||\leqslant Ch^2.
$$

Therefore,

$$
|||\mathbf{u}-\mathbf{u}_h|||\leqslant|||\mathbf{u}-\Pi\mathbf{u}|||+|||\Pi\mathbf{u}-\mathbf{u}_h|||\leqslant C(h^2+\|\Pi\mathbf{u}-\mathbf{u}_h\|)
$$

and the superconvergence results from Theorems 3.1 and 4.2 hold for $|||\mathbf{u}-\mathbf{u}_h|||$ as well. We also report the velocity error in the discrete $L^\infty$-norm $|||\mathbf{v}|||_\infty=\max_e\mathbf{v}\cdot\nu_e(m_e)$. The flux error is computed in the discrete $L^2(\Gamma)$-norm

$$
|||\mathbf{v}\cdot\nu|||_\Gamma^2=\sum_{e\in\Gamma}|e|(\mathbf{v}\cdot\nu_e)^2(m_e).
$$

The pressure error is computed in the discrete $L^2$-norm

$$
|||w|||^2=\sum_{E\in\mathcal{T}_h}|E|w^2(m_E),
$$

where $m_E$ is the center of mass of element $E$. Since $|||p-Q_hp|||\leqslant Ch^2$, $|||p-p_h|||$ is also superconvergent.

The convergence rates are established by running each test case on five (four for Examples 5.4 and 5.5) levels of grid refinement and computing a least squares fit to the error. The initial mesh on each block is uniform (shown on Fig. 2) and the initial mortar grids on all interfaces are given in Table 1. The interior subdomains $\Omega_i'$ are

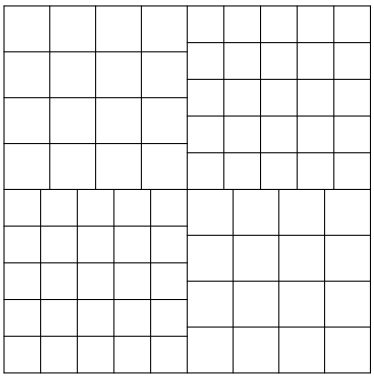

**Fig. 2.** Initial grid.

**Table 1**
Initial number of elements in mortar grids

| Mortar | 1 | 2 | 3 |
|---|---|---|---|
| Elements | 3 | 3 | 1 |

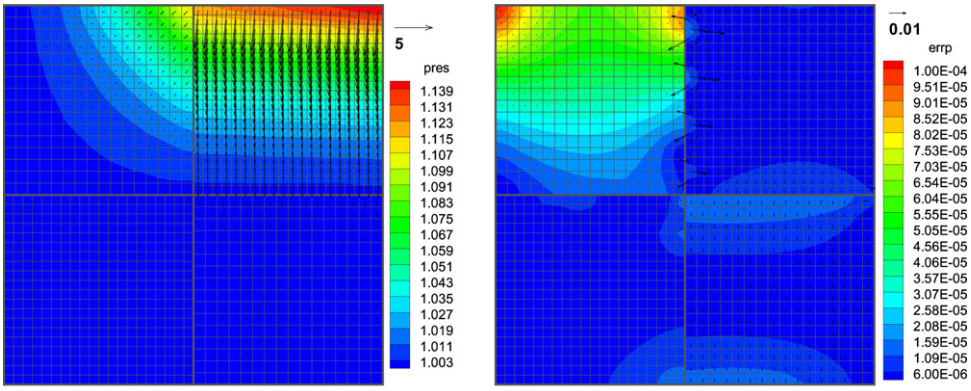


**Fig. 3.** Solution and error (magnified) with mortar 1 for Example 5.1.

chosen on the initial mesh to have a one-element border and are kept fixed during the mesh refinement. The boundary conditions are Dirichlet on the left and right edge and Neumann on the rest of the boundary. In all tests except the fourth one we solve problems with known analytical solutions.

**Example 5.1.** We choose permeability

$$K = \begin{cases} I, & 0 \leqslant x < 1/2 \\ 10 * I, & 1/2 < x \leqslant 1 \end{cases}$$

**Table 2**
Convergence rates for Example 5.1

| Mortar | $\|\|\|(\mathbf{u}-\mathbf{u}_h)\cdot\nu\|\|\|_\Gamma$ | $\|\|\|p-p_h\|\|\|$ | $\|\|\|\mathbf{u}-\mathbf{u}_h\|\|\|$ | | $\|\|\|\mathbf{u}-\mathbf{u}_h\|\|\|_\infty$ | |
|---|---|---|---|---|---|---|
| | | | $\Omega$ | Int. | $\Omega$ | Int. |
| 1 | 1.00 | 1.98 | 1.79 | 2.01 | 0.87 | 1.98 |
| 2 | 1.14 | 1.99 | 1.97 | 1.99 | 1.41 | 1.97 |
| 3 | 0.25 | 1.92 | 1.68 | 2.00 | 0.76 | 1.96 |

**Table 3**
Convergence rates for Example 5.2

| Mortar | $\|\|\|(\mathbf{u}-\mathbf{u}_h)\cdot\nu\|\|\|_\Gamma$ | $\|\|\|p-p_h\|\|\|$ | $\|\|\|\mathbf{u}-\mathbf{u}_h\|\|\|$ | | $\|\|\|\mathbf{u}-\mathbf{u}_h\|\|\|_\infty$ | |
|---|---|---|---|---|---|---|
| | | | $\Omega$ | Int. | $\Omega$ | Int. |
| 1 | 1.30 | 2.00 | 1.46 | 1.99 | 0.96 | 1.89 |
| 2 | 1.21 | 2.00 | 1.46 | 1.98 | 0.97 | 1.88 |
| 3 | 0.05 | 1.94 | 0.75 | 2.03 | 0.25 | 1.99 |

and the pressure

$$p(x,y) = \begin{cases} x^2y^3 + \cos(xy), & 0 \leqslant x < 1/2 \\ \left(\frac{2x+9}{20}\right)^2 y^3 + \cos\left(\frac{2x+9}{20}y\right), & 1/2 < x \leqslant 1 \end{cases}$$

is chosen to be continuous and to have continuous normal flux at $x = 1/2$. Note that the solution is smooth in each subdomain. Plots of the computed solution and the numerical error for Example 5.1 using mortar 1 are shown in Fig. 3. The plots for all examples are on the third level of grid refinement, except for Example 5.5, where the plots are on the second level of refinement. As shown in Table 2, the interior velocity error is superconvergent of order $\mathcal{O}(h^2)$ and most of the error occurs near the interfaces, as it can be seen from the flux error. The pressure error is also $\mathcal{O}(h^2)$-superconvergent. The results for the mortar method are as predicted by the theory and the results for the non-mortar method are approximately $\mathcal{O}(h^{1/2})$ better than the theoretical results.

**Example 5.2.** In this example, we test a problem with a discontinuous full tensor

$$K = \begin{cases} \begin{pmatrix} 2 & 1 \\ 1 & 2 \end{pmatrix}, & 0 \leqslant x < 1/2 \\ I, & 1/2 < x \leqslant 1 \end{cases}$$

and pressure

$$p(x,y) = \begin{cases} xy, & 0 \leqslant x \leqslant 1/2 \\ xy + (x - 1/2)(y + 1/2), & 1/2 \leqslant x \leqslant 1. \end{cases}$$

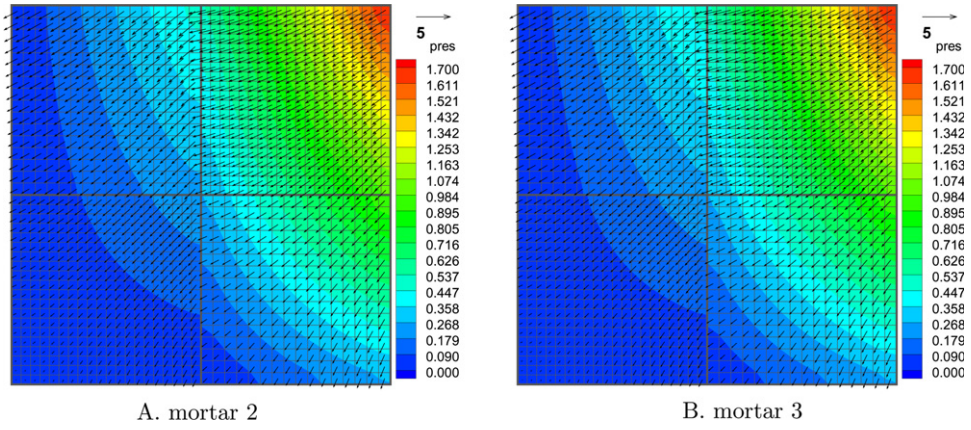


**Fig. 4.** Computed pressure and velocity for Example 5.2.

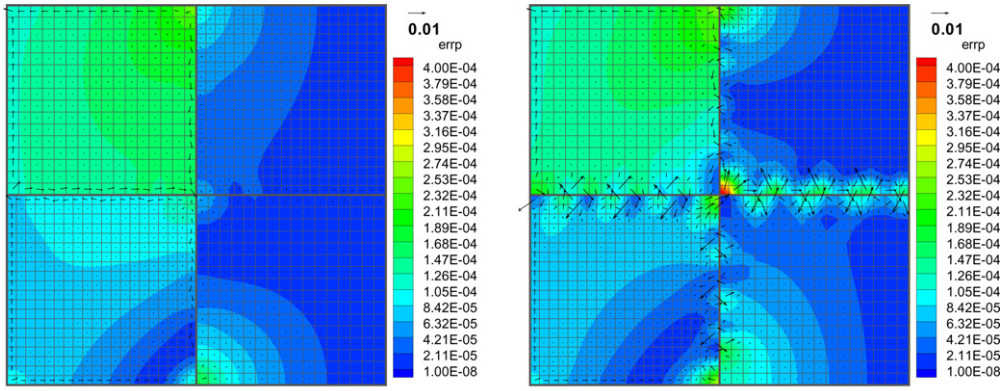


**Fig. 5.** Computed pressure and velocity error (magnified) for Example 5.2.

The convergence rates for Example 5.2 are given in Table 3 and confirm the theory. The computed pressure and velocity using the mortar and the non-mortar methods are shown in Fig. 4. Although the two solutions look the same, the velocity error along the interfaces is larger for the non-mortar method, as it can be seen in Fig. 5 where magnified numerical error is shown.

**Example 5.3.** In the third example, we test non-uniform grids. We solve a problem with a known analytical solution

$$p(x,y) = x^3y^4 + x^2 + \sin(xy)\cos(y)$$

and a diagonal tensor coefficient

$$K = \begin{pmatrix} (x+1)^2 + y^2 & 0 \\ 0 & (x+1)^2 \end{pmatrix}.$$

The initial grid is constructed from the grid on Fig. 2 via the mapping

$$x = \begin{cases} \xi + 0.05\sin(4\pi\xi)\cos(1.5\pi\xi), & 0 \leqslant \eta \leqslant 1/2, \\ \xi + 0.05\sin(4\pi\xi)\cos(0.3\pi\xi), & 1/2 \leqslant \eta \leqslant 1, \end{cases}$$

$$y = \begin{cases} \eta - 0.03\sin(12\pi\eta), & 0 \leqslant \xi \leqslant 1/2, \\ \eta - 0.05\sin(6\pi\eta)\cos(1.5\pi\eta), & 1/2 \leqslant \xi \leqslant 1, \end{cases}$$

where $\xi, \eta \in [0,1]$, and is refined uniformly for subsequent levels. For mortar 2 we have started with a coarser mortar grid (two elements per mortar interface) in order to satisfy the stability condition (2.28). The convergence rates are given in Table 4. As in the first two examples with uniform grids, the obtained convergence rates are in the accordance with the theory. Plots of the computed solution and the numerical error for Example 5.3 using mortar 2 are shown in Fig. 6.

It is evident from the first three examples that the error in the case of non-matching grids and piecewise smooth solutions occurs mainly along the interfaces and superconvergence is preserved in the interior.

**Table 4**
Convergence rates for Example 5.3

| Mortar | $\|\|\|(\mathbf{u}-\mathbf{u}_h)\cdot\nu\|\|\|_\Gamma$ | $\|\|\|p-p_h\|\|\|$ | $\|\|\|\mathbf{u}-\mathbf{u}_h\|\|\|$ | | $\|\|\|\mathbf{u}-\mathbf{u}_h\|\|\|_\infty$ | |
|---|---|---|---|---|---|---|
| | | | $\Omega$ | Int. | $\Omega$ | Int. |
| 1 | 1.41 | 1.99 | 1.79 | 2.00 | 1.13 | 1.90 |
| 2 | 1.15 | 1.99 | 1.69 | 2.01 | 1.14 | 2.02 |
| 3 | 0.69 | 1.82 | 1.22 | 1.98 | 0.25 | 1.81 |

**Example 5.4.** In this example, we test a problem with a singularity due to a cross-point discontinuity in the permeability. In this test, analytical solution is not available. Instead, a fine grid solution is used to calculate the errors on all coarser grids. We test both matching and non-matching grids. The finest grid in the case of matching grids is $128 \times 128$. The finest non-matching and mortar grids are shown in Table 6. The permeability tensor is $K = a(x,y)I$, where

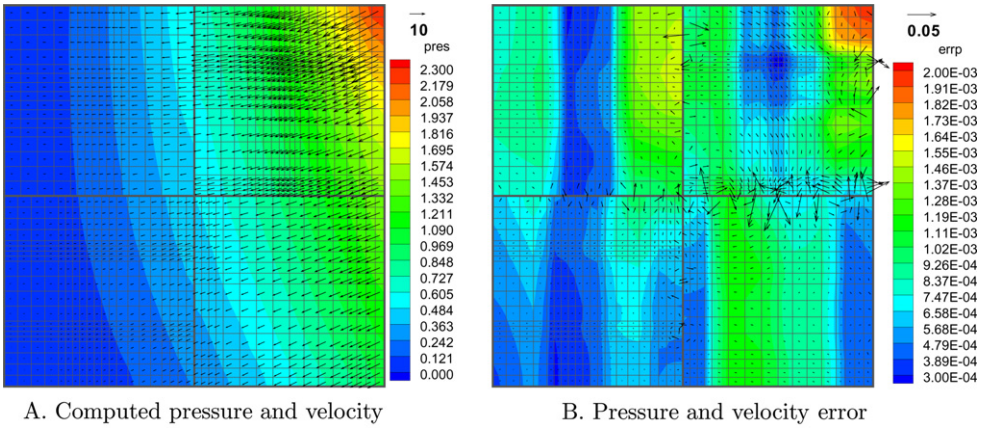


**Fig. 6.** Solution and error (magnified) with mortar 2 for Example 5.3.

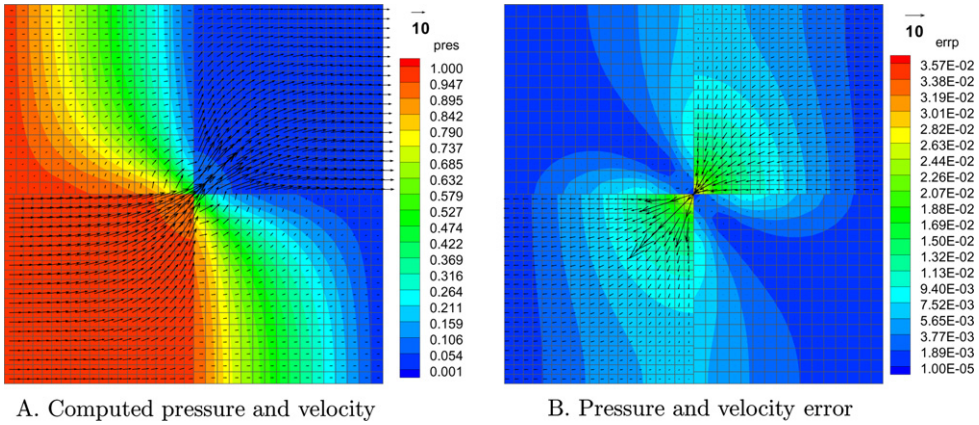


**Fig. 7.** Solution and error (magnified) with mortar 1 for Example 5.4.

$$a(x,y) = \begin{cases} 100, & \text{if } x < 1/2,\ y < 1/2 \text{ or } x > 1/2,\ y > 1/2 \\ 1, & \text{otherwise.} \end{cases}$$

$L^\infty$-errors are not reported since the true velocity is not in $L^\infty(\Omega)$. As the results show (Fig. 7, Table 5), the error due to the strong singularity at the cross-point $(1/2, 1/2)$ dominates the interface error and pollutes the solution in a large part of the domain. As a result, there is no superconvergence even in the interior. The rate of convergence for the interior velocity error is of order $\mathcal{O}(h^{3/4})$. In this case local grid refinement near this cross-point is needed to control the error [32].

**Example 5.5.** Next, we test a three dimensional problem with a full permeability tensor

**Table 5**
Convergence rates for Example 5.4

| Mortar | $\|\|\|(\mathbf{u}-\mathbf{u}_h)\cdot\nu\|\|\|_\Gamma$ | $\|\|\|p-p_h\|\|\|$ | $\|\|\|\mathbf{u}-\mathbf{u}_h\|\|\|$ | |
|---|---|---|---|---|
| | | | $\Omega$ | Int. |
| 0 | 0.18 | 0.67 | 0.60 | 0.74 |
| 1 | 0.18 | 0.68 | 0.61 | 0.74 |
| 2 | 0.14 | 0.68 | 0.60 | 0.74 |
| 3 | 0.16 | 0.68 | 0.62 | 0.75 |

**Table 6**
Finest grids for Example 5.4

| *A. Finest non-matching grids* | | *B. Mortar grids* | | | |
|---|---|---|---|---|---|
| $64 \times 64$ | $80 \times 80$ | Mortar | 1 | 2 | 3 |
| $80 \times 80$ | $64 \times 64$ | Elements | 48 | 48 | 16 |

**Table 7**
Convergence rates for Example 5.5

| Mortar | $\|\|\|(\mathbf{u}-\mathbf{u}_h)\cdot\nu\|\|\|_\Gamma$ | $\|\|\|p-p_h\|\|\|$ | $\|\|\|\mathbf{u}-\mathbf{u}_h\|\|\|$ | | $\|\|\|\mathbf{u}-\mathbf{u}_h\|\|\|_\infty$ | |
|---|---|---|---|---|---|---|
| | | | $\Omega$ | Int. | $\Omega$ | Int. |
| 1 | 1.09 | 2.00 | 1.63 | 2.02 | 0.62 | 1.97 |
| 2 | 1.32 | 2.00 | 1.75 | 1.95 | 0.86 | 1.71 |
| 3 | 0.28 | 1.98 | 0.81 | 2.05 | 1.58 | 1.74 |

**Table 8**
Convergence rates for Example 5.6

| Mortar | $\|\|\|(\mathbf{u}-\mathbf{u}_h)\cdot\nu\|\|\|_\Gamma$ | $\|\|\|p-p_h\|\|\|$ | $\|\|\|\mathbf{u}-\mathbf{u}_h\|\|\|$ | | $\|\|\|\mathbf{u}-\mathbf{u}_h\|\|\|_\infty$ | |
|---|---|---|---|---|---|---|
| | | | $\Omega$ | Int. | $\Omega$ | Int. |
| 1 | 1.38 | 1.99 | 1.53 | 1.98 | 1.02 | 1.96 |
| 2 | 1.30 | 1.99 | 1.53 | 1.98 | 1.02 | 1.96 |
| 3 | 0.05 | 1.94 | 0.69 | 1.98 | 0.15 | 1.95 |

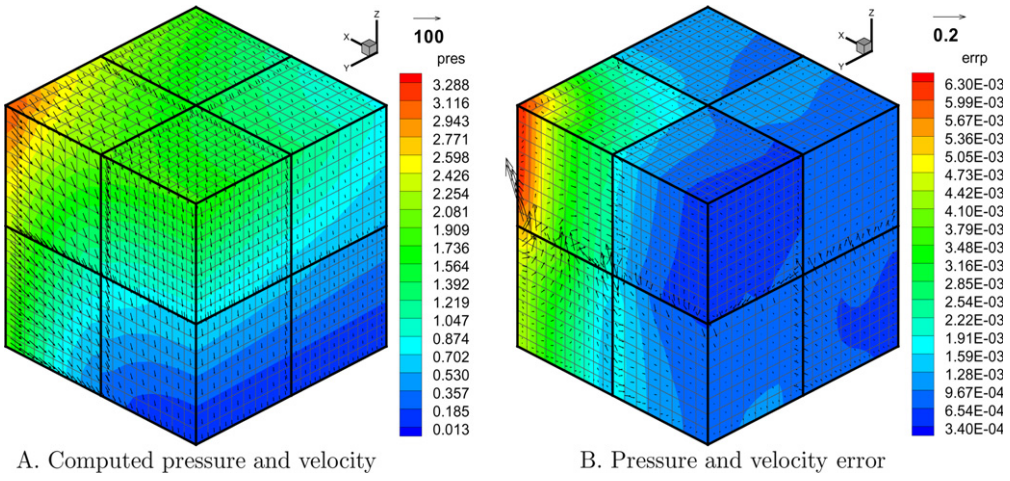


**Fig. 8.** Solution and error (magnified) with mortar 2 for Example 5.5.

$$K = \begin{pmatrix} x^2 + (y+2)^2 & 0 & \cos(xy) \\ 0 & z^2 + 2 & \sin(yz) \\ \cos(xy) & \sin(yz) & (y+3)^2 \end{pmatrix}$$

and pressure

$$p(x,y,z) = x^4y^3 + x^2 + yz^2 + \cos(xy)\sin(z).$$

Plots of the computed solution and the numerical error for Example 5.5 using mortar 2 are shown in Fig. 8. The convergence rates are given in Table 7, again confirming the theoretical results.

**Example 5.6.** In the last two examples, we test quadrilateral grids on irregular domains. We choose permeability and pressure as in Example 5.2. In this example, the computational grids are constructed from the grid on Fig. 2 and its uniform refinements via the mapping

$$x = \xi + .06\cos(\pi\xi) * \cos(\pi\eta), \quad y = \eta - .1\cos(\pi\xi) * \cos(\pi\eta),$$

where $\xi, \eta \in [0,1]$. Note that the resulting quadrilateral grids are $h^2$-uniform. The convergence rates are given in Table 8. In calculating the rates, only the two finest levels were used due to inexact computation of the errors, which affects the results on coarse grids. Just as for the case of affine elements, the interior velocity is superconvergent of order $\mathcal{O}(h^2)$ and most of the error occurs near the interfaces. The computed solution and error in pressure and velocity for Example 5.6 using mortar 2 are shown in Figs. 9A and 10A.

**Example 5.7.** In this example, the mapping used to generate the domain and the grids is

$$x = \xi + .03\cos(3\pi\xi) * \cos(3\pi\eta),$$
$$y = \eta - .04\cos(3\pi\xi) * \cos(3\pi\eta).$$

The results for Example 5.7 are in Table 9, Figs. 9B and 10B.

Comparing the numerical errors for Examples 5.6 and 5.7, we observe that although rougher mapping introduces larger error due to element distortion, interior velocity superconvergence is still obtained.

Summarizing the test results in Section 5, we conclude that in smooth cases the numerical error due to the non-matching grids in both the mortar and the non-mortar methods is restricted to a small region around the interfaces and superconvergence is preserved in the interior. For singular solutions superconvergence is not observed, although the interior velocity error is better than the velocity error calculated over the whole domain. The results in this case indicate the need for *a posteriori* error estimates and adaptive mesh refinement near the points of singularity to increase the overall accuracy of the solution.

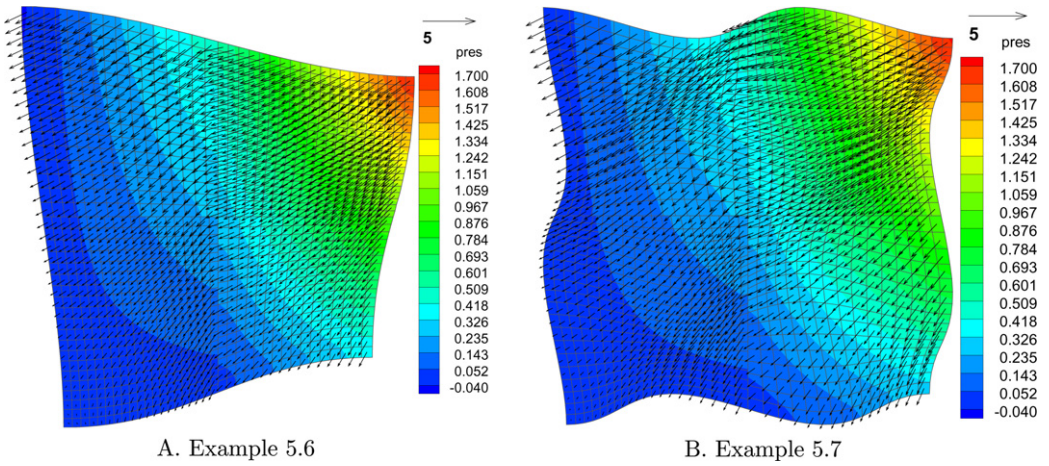


**Fig. 9.** Computed pressure and velocity with mortar 2.

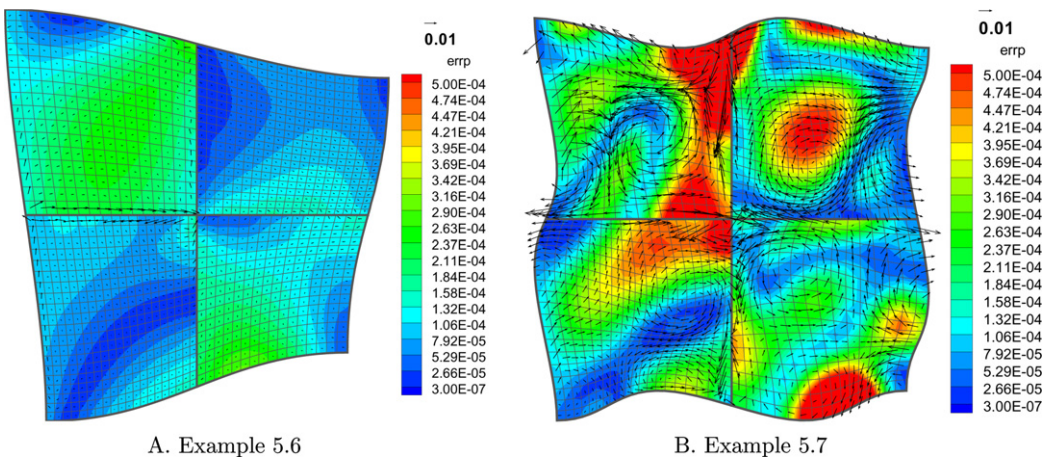


**Fig. 10.** Computed pressure and velocity error (magnified) with mortar 2.

**Table 9**
Convergence rates for Example 5.7

| Mortar | $\|\|\|(\mathbf{u}-\mathbf{u}_h)\cdot\nu\|\|\|_\Gamma$ | $\|\|\|p-p_h\|\|\|$ | $\|\|\|\mathbf{u}-\mathbf{u}_h\|\|\|$ | | $\|\|\|\mathbf{u}-\mathbf{u}_h\|\|\|_\infty$ | |
|---|---|---|---|---|---|---|
| | | | $\Omega$ | Int. | $\Omega$ | Int. |
| 1 | 1.59 | 2.01 | 1.70 | 1.97 | 0.84 | 1.95 |
| 2 | 1.58 | 2.01 | 1.70 | 1.97 | 0.84 | 1.95 |
| 3 | 0.10 | 1.99 | 1.36 | 1.94 | 0.78 | 1.95 |

## Acknowledgement

This work was partially supported by the NSF Grants DMS 0411694 and DMS 0620402 and the DOE Grant DE-FG02-04ER25618.

## References

[1] T. Arbogast, L.C. Cowsar, M.F. Wheeler, I. Yotov, Mixed finite element methods on non-matching multiblock grids, SIAM J. Numer. Anal. 37 (2000) 1295–1315.
[2] T. Arbogast, M.F. Wheeler, I. Yotov, Mixed finite elements for elliptic problems with tensor coefficients as cell-centered finite differences, SIAM J. Numer. Anal. 34 (1997) 828–852.
[3] T. Arbogast, I. Yotov, A non-mortar mixed finite element method for elliptic problems on non-matching multiblock grids, Comput. Methods Appl. Mech. Engrg. 149 (1997) 255–265.
[4] D. Arnold, F. Brezzi, Mixed and non-conforming finite element methods: implementation, post-processing and error estimates, Math. Model. Numer. Anal. 19 (1985) 7–35.
[5] D.N. Arnold, D. Boffi, R.S. Falk, Quadrilateral *H*(div) finite elements, SIAM J. Numer. Anal. 42 (2005) 2429–2451 (electronic).
[6] F. Ben Belgacem, The mortar finite element method with Lagrange multiliers, Numer. Math. 84 (1999) 173–197.
[7] C. Bernardi, Y. Maday, A.T. Patera, A new nonconforming approach to domain decomposition: the mortar element method, in: H. Brezis, J.L. Lions (Eds.), Nonlinear Partial Differential Equations and Their Applications, Longman Scientific & Technical, UK, 1994.
[8] F. Brezzi, J. Douglas Jr., R. Duràn, M. Fortin, Mixed finite elements for second order elliptic problems in three variables, Numer. Math. 51 (1987) 237–250.
[9] F. Brezzi, J. Douglas Jr., M. Fortin, L.D. Marini, Efficient rectangular mixed finite elements in two and three space variables, RAIRO Model. Math. Anal. Numèr. 21 (1987) 581–604.
[10] F. Brezzi, J. Douglas Jr., L.D. Marini, Two families of mixed elements for second order elliptic problems, Numer. Math. 88 (1985) 217–235.
[11] F. Brezzi, M. Fortin, Mixed and Hybrid Finite Element Methods, Springer-Verlag, New York, 1991.
[12] Z. Chen, J. Douglas Jr., Prismatic mixed finite elements for second order elliptic problems, Calcolo 26 (1989) 135–148.
[13] P.G. Ciarlet, The finite element method for elliptic problems, Studies in Mathematics and its Applications, vol. 4, North-Holland, Amsterdam, 1978.
[14] J. Douglas Jr., F.A. Milner, Interior and superconvergence estimates for mixed methods for second order elliptic problems, RAIRO Model. Math. Anal. Numer. 19 (1985) 397–428.
[15] R. Durán, Superconvergence for rectangular mixed finite elements, Numer. Math. 58 (1990) 287–298.
[16] R. Ewing, R. Lazarov, T. Lin, Y. Lin, Mortar finite volume element approximations of second order elliptic problems, East-West J. Numer. Math. 8 (2000) 93–110.
[17] R.E. Ewing, R.D. Lazarov, J. Wang, Superconvergence of the velocity along the Gauss lines in mixed finite element methods, SIAM J. Numer. Anal. 28 (1991) 1015–1029.
[18] R.E. Ewing, M. Liu, J. Wang, Superconvergence of mixed finite element approximations over quadrilaterals, SIAM J. Numer. Anal. 36 (1999) 772–787.
[19] R. Glowinski, M.F. Wheeler, Domain decomposition and mixed finite element methods for elliptic problems, in: R. Glowinski, G.H. Golub, G.A. Meurant, J. Periaux (Eds.), First International Symposium on Domain Decomposition Methods for Partial Differential Equations, SIAM, Philadelphia, 1988, pp. 144 – 172.
[20] P. Grisvard, Elliptic problems in nonsmooth domains, Monographs and Studies in Mathematics, vol. 24, Pitman (Advanced Publishing Program), Boston, MA, 1985.
[21] Y.A. Kuznetsov, M.F. Wheeler, Optimal order substructuring preconditioners for mixed finite element methods on non-matching grids, East-West J. Numer. Math. 3 (1995) 127–143.
[22] J.L. Lions, E. Magenes, Non-homogeneous Boundary Value Problems and Applications, vol. 1, Springer-Verlag, 1972.
[23] L. Marcinkowski, The mortar element method with locally nonconforming elements, BIT 39 (1999) 716–739.
[24] M. Nakata, A. Weiser, M.F. Wheeler, Some superconvergence results for mixed finite element methods for elliptic problems on rectangular domains, in: J.R. Whiteman (Ed.), The Mathematics of Finite Elements and Applications V, Academic Press, London, 1985, pp. 367–389.
[25] J.C. Nedelec, Mixed finite elements in $R^3$, Numer. Math. 35 (1980) 315–341.
[26] G. Pencheva, I. Yotov, Balancing domain decomposition for mortar mixed finite element methods on non-matching grids, Numer. Linear Algebra Appl. 10 (2003) 159–180.
[27] R.A. Raviart, J.M. Thomas, A mixed finite element method for second order elliptic problems, in: Mathematical Aspects of the Finite Element Method, Lecture Notes in Mathematics, vol. 606, Springer-Verlag, New York, 1977, pp. 292–315.
[28] J.E. Roberts, J.-M. Thomas, Mixed and hybrid methods, in: P.G. Ciarlet, J. Lions (Eds.), Handbook of Numerical Analysis, vol. II, Elsevier Science Publishers B.V., 1991, pp. 523–639.
[29] J.M. Thomas, Sur l'analyse numerique des methodes d'elements finis hybrides et mixtes, Ph.D. Thesis, Sciences Mathematiques, à l'Universite Pierre et Marie Curie, 1977.
[30] J. Wang, T.P. Mathew, Mixed finite element method over quadrilaterals, in: I.T. Dimov, B. Sendov, P. Vassilevski (Eds.), Conference on Advances in Numerical Methods and Applications, World Scientific, River Edge, NJ, 1994, pp. 203–214.
[31] J.A. Wheeler, M.F. Wheeler, I. Yotov, Enhanced velocity mixed finite element methods for flow in multiblock domains, Comput. Geosci. 6 (2002) 315–332.
[32] M.F. Wheeler, I. Yotov, A posteriori error estimates for the mortar mixed finite element method, SIAM J. Numer. Anal. 43 (2005) 1021–1042.
[33] B.I. Wohlmuth, A mortar finite element method using dual spaces for the Lagrange multiplier, SIAM J. Numer. Anal. 38 (2000) 989–1012.
[34] I. Yotov, Mixed finite element methods for flow in porous media, Ph.D. Thesis, Rice University, Houston, Texas, 1996. TR96-09, Dept. Comp. Appl. Math., Rice University and TICAM Report 96-23, University of Texas at Austin.